Computational Modeling of a Molten Salt Reactor

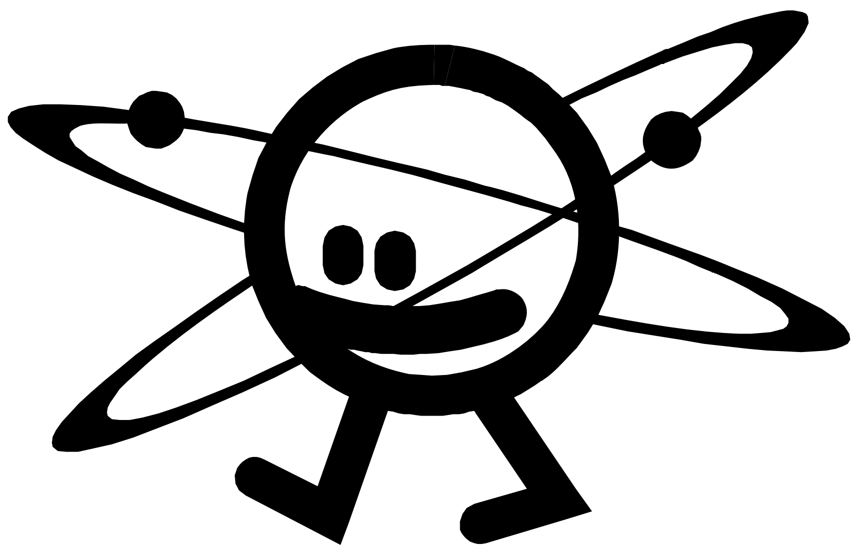

Author: Gert Jan Auwerda
Supervisor: Danny Lathouwers
TU Delft
May 28, 2007

Summary

In this report the computational modeling of a molten salt reactor (MSR) is described and the subsequent testing of that model. The testing was done by comparing computational results from the model with experimental results done in various tests at the Oak Ridge National Laboratory (ORNL) during the Molten Salt Reactor Experiment (MSRE). The experimental MSR from the MSRE ran from 1965 until 1969. The results were also compared with results from another computational model, the EDF core, which used the same basic physical model as implemented in the present model.

In a MSR the fuel for the fission process is dissolved in a fluid salt, which is pumped around in a primary loop through the reactor core and through a heat exchanger. A benefit is that an online processing plant can be included in the primary loop to add new fuel to the fuel-salt or remove fission products from the fuel-salt that are harmful to the fission process, without the need to shut down the reactor.

For the physical model a point kinetic code was chosen. Since in an MSR the fuel is moving, so are the precursors, and the basic point kinetic model had to be adjusted including the precursor concentration as a function of the z position, the axial position in the primary loop. Only axial variations of any variables were modeled in the code, and any radial dependency was neglected. The fuel flow-rate was modeled as a plug flow. The fission shape was used to describe the z location at which precursors are created inside the core and the adjoint flux shape was used as a weight factor for the delayed neutrons emitted by the precursors, as a function of z. The core geometry was modeled as a uniform cylinder with homogeneous distribution of salt and graphite (the moderator) throughout the core. The model calculated the total number of neutrons inside the core, the precursor concentration as a function of z, the fuel-salt temperature as a function of z and the reactivity change due to the fuel and graphite temperatures. It was assumed that the graphite temperature was the same as that of the fuel-salt.

In the discretization of the model, the geometry was discretized using a finite volume method, in which the primary loop was divided in volume elements all with the same length Δz. For the discretization of the different functions, in space finite volumes with an upwind model was used, and implicit time discretization was used. The calculation in each time step of the number of neutrons and the precursor concentrations for each precursor group were separated, to lower the calculation time.

In the first benchmark the reactivity lost due to fuel motion was calculated. This benchmark was also used to choose which fission and adjoint flux shapes (flat or sine shape) gave the best calculation results and should be used in the rest of the benchmarks. The computational model gave results 10 to 20% too high. The fact that the fission and adjoint flux shapes were only rough choices, instead of calculated, and more important the ignoring of any radial dependency were probably the biggest cause of these deviations.

The second benchmark calculated the reactivity that had to be inserted to keep the reactor core critical during the fuel-pump start-up transient. The model followed the transient

nicely, apart from an initial overshoot which was too big and fluctuations in the reactivity inserted that were not observed in the MSRE data, but both were observed in the results from the EDF code. These differences were most likely due to a strong simplification in the flow model, ignoring any mixing of the fuel-salt in the fuel pump or upper and lower plenums of the reactor core, and differences in flow speed in the graphite lattice inside the core.

The third benchmark detailed the reactivity that had to be inserted to keep the core critical during the fuel-pump shut-down transient. The computational model followed almost exactly the measured reactivity inserted in the MSRE as well as that calculated by the EDF code.

The last benchmark was the only benchmark not at zero-power. This means that as opposed to the other three benchmarks, now power was generated inside the reactor core and the temperature of the fuel-salt was calculated, instead of kept constant. Also the temperature feedback on the reactivity due to changing fuel-salt temperatures was included. This benchmark detailed a natural convection transient. In this transient the fuel flow was entirely driven by natural convection. This was generated due to the temperature difference over the core. In the transient the fuel-salt temperature at the core inlet was changed in time, which due to temperature feedback on reactivity caused the reactor power to rise, and due to a higher temperature difference over the reactor core caused a higher fuel-salt flow-speed. In the model the core inlet temperature was given as a function of time, as well as the fuel-salt flow-speed $g(t)$, since it would be very complicated to calculate $g(t)$ from the temperature difference over the core. The calculated power during the natural convection transient as a function of time followed the shape of that measured during the MSRE almost exactly. The power showed strong fluctuations around its equilibrium value in the first 100 minutes of the transient, which were not observed in the results from the MSRE, and the calculated power was 20% higher than that measured during the MSRE. The strong fluctuations were probably a result from the simplifications in the flow model, just as in the second benchmark. A more diverse fuel-flow pattern in the reactor core and plenums would dampen these fluctuations. The calculated power was too high because the fuel-salt and graphite temperatures were not calculated separately in the computational model. Because the fuel-salt is also the coolant in an MSR, in reality the graphite temperature will be higher than the fuel temperature. Since both the graphite and the fuel-salt have a negative temperature feedback coefficient on the reactivity, a higher graphite temperature would mean that the fuel temperature would be lower at steady state with the reactor core critical. Since the fuel flow-rate and inlet temperature were fixed in the natural convection transient, a lower average fuel temperature in the reactor core would result in less power generated inside the core.

From the results from these four benchmark, it was concluded that the developed computational model is well suited to simulate a molten salt reactor, for transients as well as steady state situations. But if precise numerical values are needed with a small error margin, a more detailed model is required.

Table of contents

1 Introduction

With the problems of the greenhouse effect and the depletion of fossil fuels, as well as the fact that a lot of the fossil resources left are in politically unstable areas, the need for alternative energy sources rises. Nuclear energy is such an alternative energy source, and an interesting candidate, because nuclear power plants emit no greenhouse gases. This study will focus on a specific type of nuclear power plant, the molten salt reactor (MSR).

The MSR is a generation IV reactor. Generation IV reactors are a set of theoretical nuclear reactor designs currently being researched and are expected to be available for commercial construction around 2030. The primary goals of these designs are to improve nuclear safety, improve proliferation resistance, minimize waste and nuclear resource utilization, and to decrease the cost to build and run such plants [1]. Proliferation resistance means that a reactor cannot be used to produce materials to make nuclear weapons.

In a molten salt reactor the fuel (heavy atoms like uranium-233 or -235) is dissolved in a fluoride salt, which also serves as the coolant fluid as it is pumped around. The fuel-salt mixture flows around in a primary loop through the reactor core and through a heat exchanger outside the core. Inside the core the fuel flows through channels in between graphite bars. Heat produced in the reactor core is transferred by the fuel-salt outside the core, through a heat exchanger, to a secondary coolant salt (the secondary loop), and from there through another heat exchanger to the power conversion system.

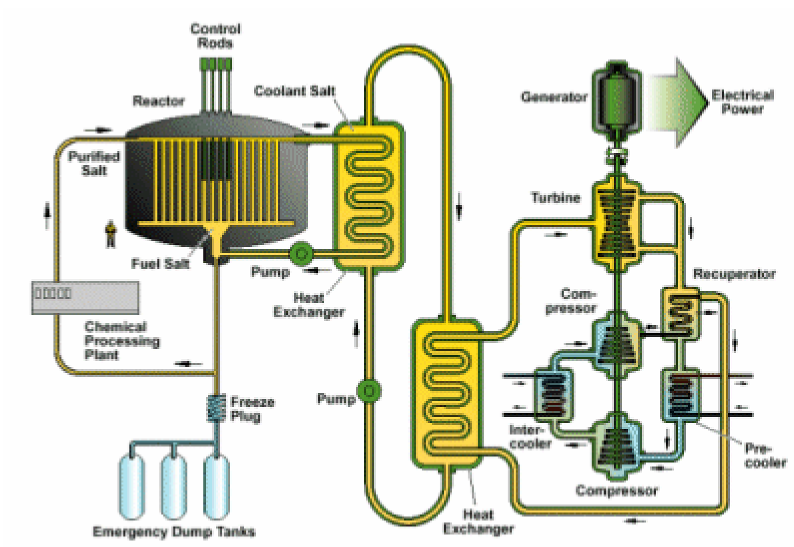

Figure 2.2: Molten salt reactor scheme [1].

All valves in the salt piping are so called freeze valves. They are made of plugs of fluoride salt frozen in flattened sections of the pipes, cooled by air. The freeze valves are kept at such a temperature that they will melt in 10 to 15 minutes when needed. A power failure will result in a drain because the valves will no longer be cooled, and the fuel-salt will flow into drain tanks beneath the core, where it is cooled by natural convection.

A benefit of circulating fuel is that a processing plant can be added to the primary loop, in which contaminating elements created in the fission process can be constantly removed from the fuel without shutting down the reactor (or elements can be added).

From 1965 to 1969, at the Oak Ridge National Laboratory (ORNL), an 8 MW molten salt reactor was operated, the molten salt reactor experiment (MSRE). The MSRE ran first with U-235 and later with U-233 fuel. During the MSRE measurements were done on various aspects of the molten salt reactor during different experiments, which are used in this report as a benchmark to compare the results of the computational model with the actual experimental results from the MSRE.

This project was executed as a bachelor thesis project for applied physics at the technical university of Delft. The goal of this project was to develop a one dimensional calculation tool to simulate the behavior of a MSR, and to test the viability of this tool.

The outline of this report is first an explanation of the basics of nuclear reactor physics, after which the general workings of a molten salt reactor are investigated. In the rest of chapter two, the physical models used to calculate the different variables of interest in the computational model are explained in detail. In the third chapter the computational modeling of first the MSR geometry and then the equations for the variables of interest is explained. This includes the time and space discretization of the physical models as well as the implementation in the computer code. The next chapter, chapter four, covers the four benchmarks used to evaluate the calculation tool, including a discussion of these results and a comparison with the measurements done in the MSRE at the Oak Ridge National Laboratory. Finally, chapter five contains a discussion and conclusion on the validity of the computational model, based on the results gained from the benchmarks, as well as several recommendations on further development of the computational tool. In Appendix A some additional calculation results are presented and Appendix B contains the numerical data used as input in the calculations, gained from data on the MSR at the MSRE. Appendix C covers some basic tests run to validate the developed calculation tool.

2 Modeling of the MSR

2.1 Introduction to nuclear reactor physics

The binding energy of the neutrons and protons in the nucleus of an atom is the energy that needs to be added to split the nucleus into its separate nucleons. Or the other way around, it is the energy that is released when the loose neutrons and protons are brought together to form the nucleus. This binding energy is, per nucleon, maximal for iron and lower for heavier and lighter nuclei. This means that if a heavy nucleus like uranium is split into two lighter nuclei, with a higher binding energy per nucleon, energy is released.

Fission of a heavy nucleus like uranium can be induced by adding a neutron to the core. This will add the binding energy of this extra neutron to the nucleus, as well as any kinetic energy of the neutron before absorption. If this is higher than a certain activation energy the nucleus will split. In the fission process the target nucleus plus one neutron is transformed into two fission products, v neutrons and approximately 200 MeV of energy. For comparison, in the combustion of 1 molecule of methane gas 8 eV of energy is released, 0.000004% of the energy released in the fission of one uranium-235 atom.

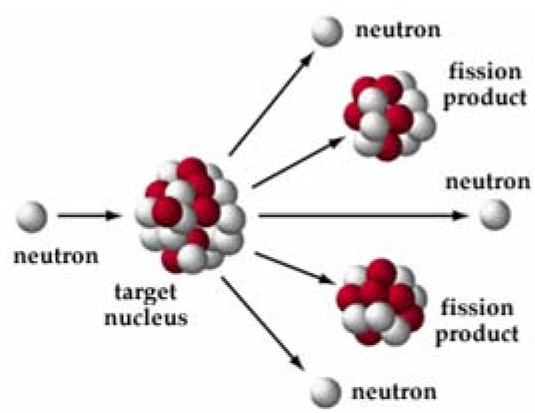

Figure 2.1: The fission process [2].

To gain power from fission you need to sustain a neutron chain fission reaction (see figure 2.2). For every fission reaction induced by a neutron you need to gain at least one new neutron that also induces fission. On average v neutrons are created per fission in the fission process and neutrons are lost when they leave the reactor core, are captured by a nucleus (fuel or other) without inducing fission, or are captured by a fissile nucleus inducing fission.

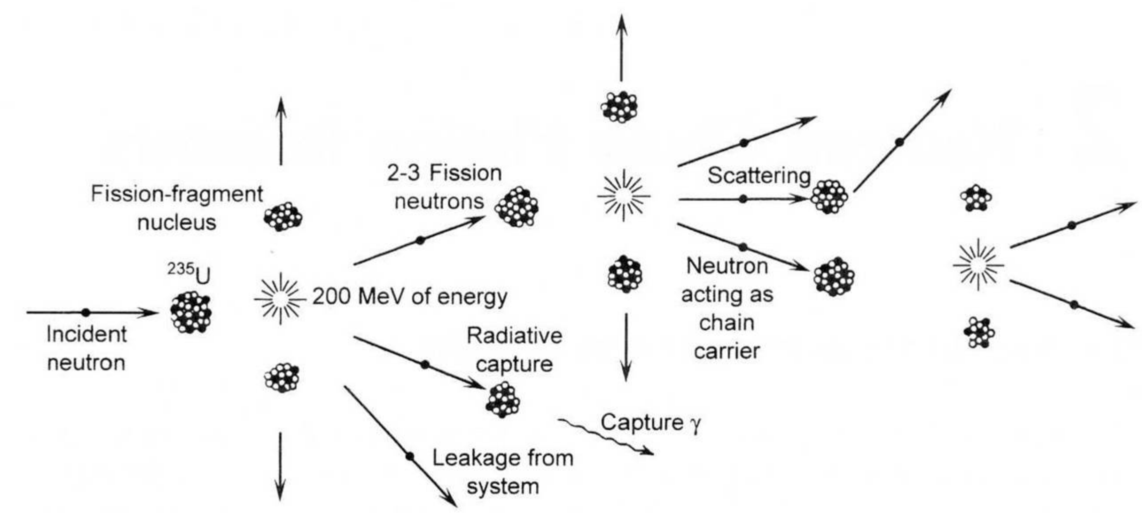

Figure 2.2: The neutron chain fission reaction process [1].

The probability that a neutron is captured by or induces fission in a certain nucleus depends on the absorption and fission cross sections of that nucleus. A nucleus with a big cross section is a 'bigger' target for neutrons than a nucleus with a small cross section. These cross sections depend on the energy (speed) of the incident neutron.

Neutrons created in the fission process have a high energy, in the order of MeV. For uranium-233 and -235 the fission cross sections are (much) larger for low energy neutrons, called thermal neutrons, with energies in the order of eV. So to maximize the probability of a neutron to induce fission in a fissile nucleus, we have to slow down the neutrons to thermal (low) energy. Neutrons slow down by scattering from other nuclei. A material which is used to slow down neutrons is called a moderator. Good moderators are materials with high scattering cross sections and very small absorption cross sections. Carbon (C) is such a material and is used in the molten salt reactor (MSR) as the moderator.

There are two sources of neutrons from the fission process, prompt neutrons and delayed neutrons. On average $\nu(1-\beta)$ prompt neutrons are directly created in the fission process, but a small fraction β of the total ν neutrons created per fission are so-called delayed neutrons. These delayed neutrons are released by the decay of certain fission products called delayed neutron precursors. This release occurs at some time after the actual fission has taken place, hence the term delayed neutrons. There emission is delayed compared to the time of the fission reaction in which their precursor is created. The number of precursors that are created depends of course on the number of fissions that takes place and the rate of fission in turn depends on the number of neutrons in the reactor core, since the neutrons induce fission.

The delayed neutron precursors can be separated into different groups (usually 6), each with its own decay constant λ_i, defined by $C_i(t) = C_i(0)\exp(-\lambda_i t)$, with $C_i(t)$ the total number of precursors of group i at time t, and a yield fraction β_i. There are on average $\nu\beta_i$

precursors of group i created per fission. The total fraction of the neutrons gained from fission that are delayed is $\beta = \Sigma\, \beta_i$.

With this information a set of equations describing the rate of change of the number of neutrons and precursors inside the reactor can be formed. These equations are called the point kinetic equations.

$$\frac{dN(t)}{dt} = \frac{\rho(t) - \beta}{\Lambda} N(t) + \sum_{i=1}^{6} \lambda_i C_i(t) \qquad (2.1.1)$$

$$\frac{dC_i(t)}{dt} = \frac{\beta_i}{\Lambda} N(t) - \lambda_i C_i(t) \qquad i = 1 \ldots 6 \qquad (2.1.2)$$

$N(t)$ is the total number of neutrons in the reactor core at time t. $C_i(t)$ is the total number of precursors of group i in the reactor core at time t. Λ is the mean generation time between the birth of a fission neutron and the subsequent absorption leading to another fission. It is the average time between two fission events in the neutron chain fission reaction.

$\rho(t)$ is the reactivity of the reactor. It describes the amount of 'extra' neutrons that are created per neutron in one fission step. To sustain the neutron chain fission reaction, at least one new neutron has to be created for every neutron that was created in the previous fission reaction. If exactly one new neutron is created per neutron from the previous reaction, the number of neutrons stays constant and the reactivity is zero. This condition is referred to as criticality, and when this is the case the reactor core is critical. If more then one neutron is created per neutron from the previous fission step, the reactivity ρ is positive, and the total number of neutrons will increase. If fewer neutrons are created, the reactivity is negative, and the total number of neutrons will decrease in time.

The reactivity is higher if the probability that a neutron induces fission is higher and lower if the probability that a neutron is captured or leaves the reactor is higher. These probabilities depend, among other things, on the various cross sections (absorption, fission and scattering) of the materials used inside the reactor. The cross sections in turn depend, among other things, on the temperature. If the binding energy of an incident neutron plus its relative kinetic energy to a nucleus match the energy of an exited state of the compound nucleus that would be formed, the probability of capture is very large. That is, the absorption cross section has a very sharp peak at that neutron energy. These resonance peaks occur mostly in the thermal energy part of the neutron spectrum, that is, for low energy (slow moving) incident neutrons. Nuclei are always vibrating around their location. When the temperature rises, these vibrations get stronger. An incident neutron with a certain speed can now have various relative speeds (energies) as compared to the vibrating nucleus, depending on the direction and speed of the vibration of the nucleus at the moment the neutron passes the nucleus. Because of this at higher temperatures neutrons in a bigger energy range can match the resonance energy, and the resonance peaks get 'smeared out' over a broader energy interval, lowering the peak height but broadening the resonance peak. The broadening of the resonance peaks in the cross sections with rising temperature is called Doppler broadening and causes the total absorption cross sections, integrated over the whole neutron energy spectrum, to increase with temperature. Thus Doppler broadening causes the reactivity to lower when the temperature rises, introducing a negative temperature feedback coefficient on the reactivity.

A way to manually adjust the reactivity of a reactor is by control rods. A control rod is a rod inserted inside the reactor, made of a material that has large absorption cross-section. This makes it a neutron absorber. The further this rod is inserted in the reactor, the more neutrons it will absorb, thus lowering the reactivity. Extracting the control rod will lower the probability of neutrons to be absorbed, raising the reactivity of the reactor. In this way reactivity can be 'inserted' and 'withdrawn' from the reactor.

In a MSR the fuel is circulating in a primary loop and is part of the time outside the core, where, without moderation, no fission takes place. It also means that the precursors move before they decay, and will emit their delayed neutrons at a different location than where they were created, possibly outside the reactor core. Any neutrons emitted here will escape from the fuel-salt before they can cause fission and are lost to the fission process.

2.2 Geometric model

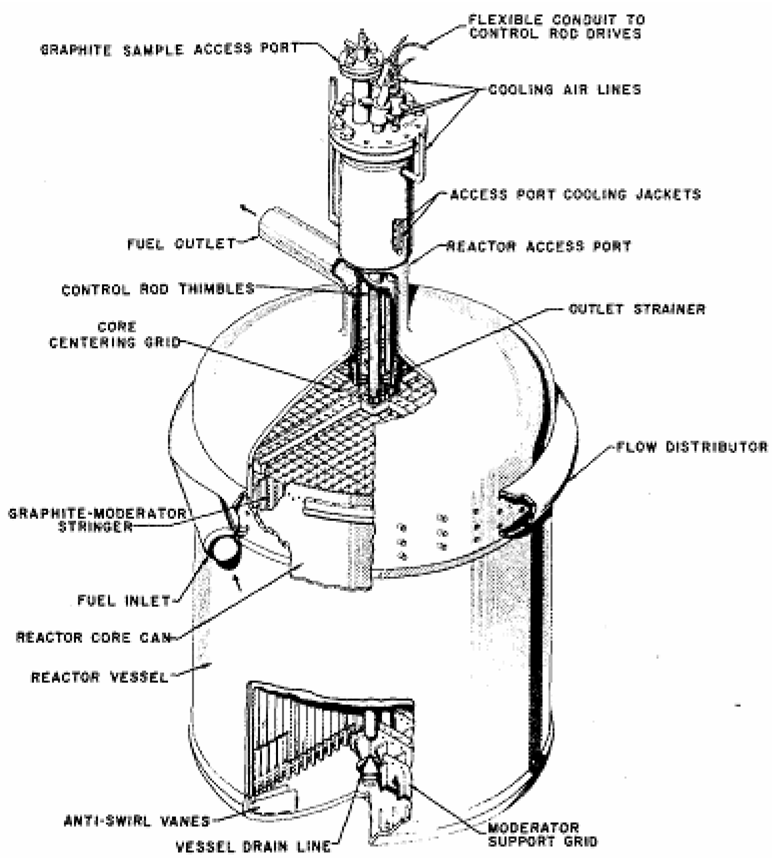

Figure 2.3: The reactor core from the MSRE [3].

A detailed figure of the core geometry used in the MSRE is depicted in figure 2.3. A schematic cross-section of the core is given in figure 2.4. In our computational tool the core was assumed homogeneous, so the core contained a homogeneous mixture of the graphite and fuel-salt. Also, the core was modeled as cylindrical and the upper and lower plenums were ignored. Tests at the ORNL and in the MOST project [4] showed that the effective core fuel volume (the fuel volume in which fission takes place) was 20.6% higher than the fuel volume in between the graphite bars, because of contributions of the delayed neutrons emitted in the lower and (particularly) upper plenum. This appears to be a consequence of the big volume fraction and long residence time of the fuel in these regions and the displacement of the equilibrium of the precursor distribution towards the upper plenum due to the fuel movement.

In the present study, the core of the MSR was modeled as a homogeneous cylindrical core of 200 cm high (120.6% of the height of the graphite matrix in the MSRE core), with a fuel volume equal to the 'effective' fuel volume observed in the MSRE project ($818.8 \cdot 10^3$ cm^3) and a total graphite mass equal to that in the MSRE core, see figure 2.4.

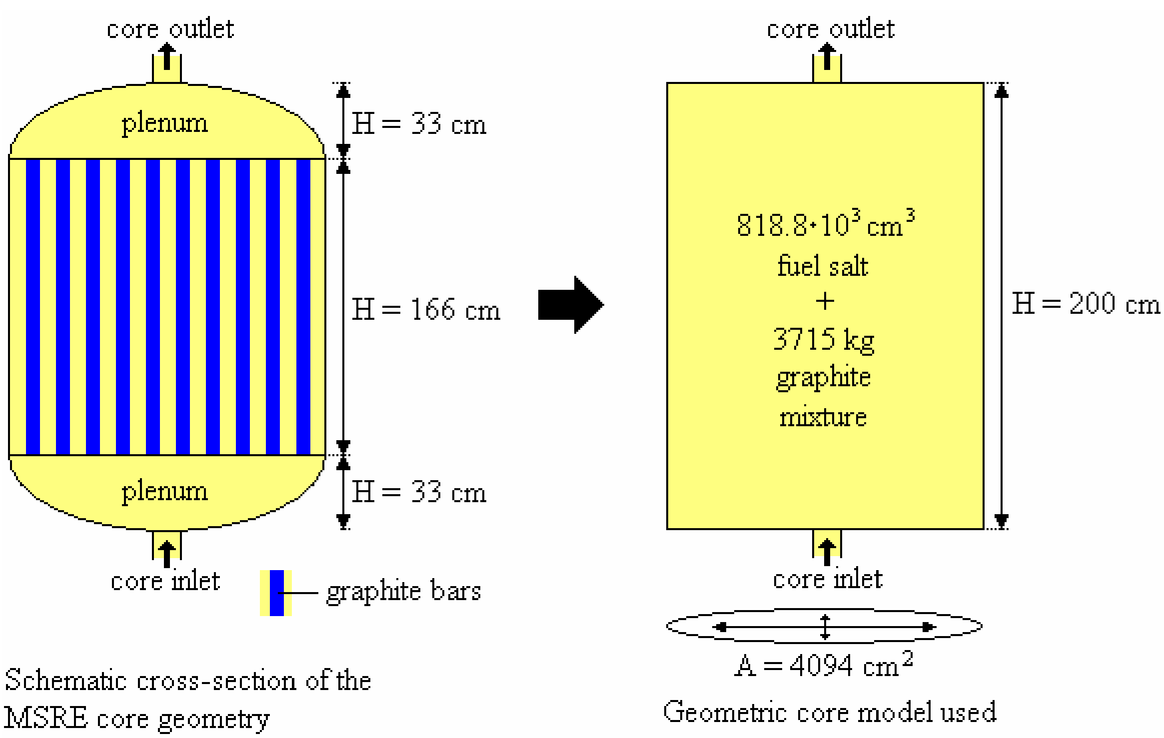

Figure 2.4: Geometry of the reactor core in the MSRE (left side) and the geometric core model used in the computational model (right side).

Inside the reactor core the neutrons are moderated and fission takes place. Outside the core there is no moderation or fission and the neutron flux is approximately zero.

No data was found detailing the geometry of the heat exchanger or the pipes between the heat exchanger and the reactor core. Only the fuel-salt volume outside the reactor core is known. The geometry outside the core is modeled as a heat exchanger and two pipes connecting the core with the heat exchanger. Volumes and lengths of the heat exchanger and the pipes are guessed and they are modeled as pipes with uniform cross-sections. The complete model of the geometry of the MSR as used in the computational model is depicted in figure 2.5.

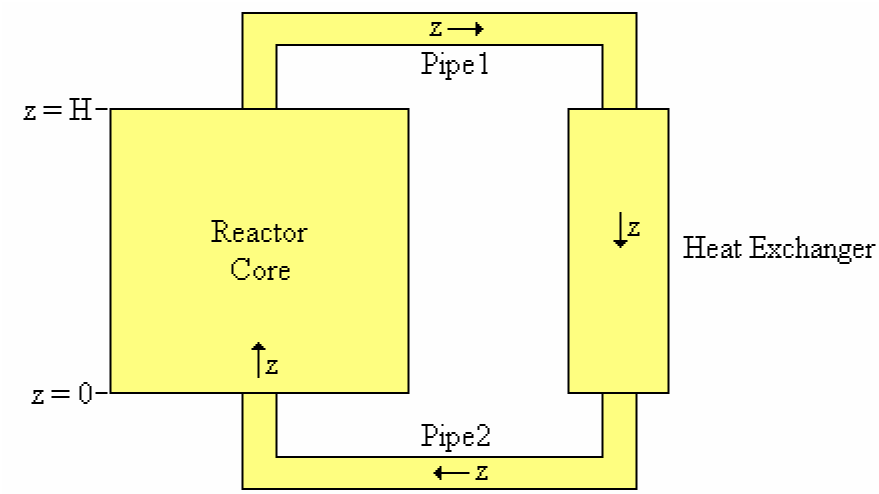

Figure 2.5: Geometrical model of the MSR used in the computational model.

2.3 Neutronics model

Next the neutron balance equations (2.1.1) and (2.1.2) were adapted for a MSR. A model using the point kinetic equations was chosen, as opposed to a neutron diffusion equation, because the point kinetic equations are much easier to solve than the diffusion equation, since they contain no explicit spatial dependence. Also, this way no cross-section data will be needed. Finally, it is very straightforward to calculate the fission power with a point kinetic model. For simplicity a model with 1 neutron energy group was chosen. As mentioned before the probabilities that neutrons are captured by or induce fission in a nucleus or scatter from a nucleus (the various cross sections) depend on the neutron energy. In a model with only 1 energy group these cross sections and other values depending on the neutron energy are averaged over the neutron energy spectrum inside the reactor. Thus for all these variables only one averaged value can be used, and only one value for the total number of neutrons inside the reactor is used.

It was assumed that all functions depending on space could be split in radial part (perpendicular to the flow direction) and an axial part (parallel to the flow direction). It was also assumed that the fuel-salt flow-speed did not vary with the radial position r (plug flow). This meant that any interaction in the axial direction z did not depend on the radial position and all functions could be modeled as only depending on the axial position z, since they could be averaged over their radial part.

Since in a MSR the fuel is moving, so are the precursors and the computational model has to keep track of their location. As can be seen from formula’s (2.1.1) and (2.1.2), only the total number of precursors inside the core is calculated. For a MSR, they will have to be adapted for usage with the precursors as a function of the axial position z. This also means the location at which precursors are formed is important, and the effect of the location where a precursor decays becomes of interest. For these the neutron flux φ is of interest.

The neutron flux describes, at a certain location, the number of neutrons passing through a sphere with cross section 1 cm^2 per second [neutrons/cm^2s]. It can also be explained as the distance traveled in cm by neutrons in a sphere with a volume of 1 cm^3 per second. The more neutron movement there is at a location, the higher the probability of an interaction with a nucleus at that location. So the higher the neutron flux the more interactions there will be and the higher the number of fission reactions. And if there are more fission reactions, more precursors will be created at that location. We are only interested in the flux shape and than only in the z dependent part of its shape. This is taken in this model as the z component of the fission shape and describes the relative amount of fission that takes place at z as compared to the total fission.

In this model, $f(z)$ (in m^{-1}), which is the z-component of the fission shape normalized to 1, is used to describe the location at which precursors are created. In our model two different shapes will be investigated. One is the flat fission shape, where the fission is uniform in the z direction throughout the reactor core. The other is a sine shaped fission shape. If you are at the border of a reactor core, neutrons can only come from one direction, since neutrons are only created inside the reactor core, while if you are at the center, neutrons will come from all directions. Thus the neutron flux will be higher at the center of a reactor core then at its border. For a homogeneous cylindrical reactor core, the z component of the neutron flux shape has a sine shape [5]. With H the height of the reactor core, these two different fission shapes $f(z)$ are given by:

$$f(z) = \left(1/H\right) / \int_0^H 1/H dz = 1/H \tag{2.3.1}$$

$$f(z) = \sin\left(\pi\left(z + \tfrac{1}{2}\lambda_{extrap}\right)\middle/H_{ex}\right) / \int_0^H \sin\left(\pi\left(z + \tfrac{1}{2}\lambda_{extrap}\right)\middle/H_{ex}\right) dz \tag{2.3.2}$$

$f(z) = 0$ outside the core. H_{ex} is the extrapolated height of the reactor core and λ_{extrap} is the distance from the core boundary at which the flux, when extrapolated beyond the core boundary, becomes zero (see (8.1.1)). These extrapolated values come from the fact that the neutron flux is not zero at the core boundary itself. There are still neutrons created inside the core that travel through the boundary and leave the core.

The effect of the location where a precursor decays depends on the probability that a neutron created at a certain location will contribute to the fission process before leaving the reactor core. This probability is zero outside the core and most likely highest in the center of the core. To describe the relative probability that a neutron created at a certain location will contribute to the fission process, the adjoint flux $\varphi^\dagger(z)$ is used. Again two different shapes are tested in this model, a flat adjoint flux shape and a sine shape. The two different adjoint fluxes are, inside the reactor core ($0 < z < H$)

$$\varphi^{\dagger}(z) = 1 \tag{2.3.3}$$

$$\varphi^{\dagger}(z) = \sin\left(\pi\left(z + \tfrac{1}{2}\lambda_{extrap}\right)\big/ H_{ex}\right) \tag{2.3.4}$$

and $\varphi^{\dagger}(z)$ is zero outside the core, since here all neutrons emitted will leave the fuel salt without causing fission.

To gain a point kinetic model which also keeps track of the z location of the precursors we start with the original point kinetic equations (2.1.1) and (2.1.2) and replace the total number of precursors $C_i(t)$ with the precursor density $C_i(z,t)$ in precursors/m^3 at location z. In (2.1.1) the number of precursors is multiplied by the area $A(z)$ perpendicular to the z direction through which the fuel-salt flows (in cm^2), multiplied by $\varphi^{\dagger}(z)$ and integrated over z before multiplied by it's decay constant λ_i to get the total number of neutrons contributing to the fission process from decaying precursors. It was divided by the integral of $f(z)\varphi^{\dagger}(z)$ over z for normalization, since the integral over z of $\varphi^{\dagger}(z) \neq 1$. In (2.1.2) the number of neutrons $N(t)$ is devided by $A(z)$ and multiplied by $f(z)$ to get the number of precursors generated from fission at location z per m^3. Also a term describing the transport of precursors due to the fuel-salt volume flow $g(z,t)$ (in cm^3/s) is added. Finally, in (2.1.1) the reactivity ρ was split in two terms. First a term describing the reactivity change due to temperature feedback, $\rho(T)$ (see section 2.5 for more details). The second term describes a reactivity change due to insertion or extraction of reactivity in the reactor by control rod movement, $\rho_{rod}(t)$. This brings us to a point kinetic model with resolution of the 1D axial precursor equations:

$$\frac{\partial N(t)}{\partial t} = \frac{\rho(T) + \rho_{rod}(t) - \beta_{eff}}{\Lambda} N(t) + \sum_{i=1}^{6} \lambda_i \frac{\int_0^H A(z) C_i(z,t) \varphi^{\dagger}(z) dz}{\int_0^H f(z) \varphi^{\dagger}(z) dz} \tag{2.3.5}$$

$$\frac{\partial C_i(z,t)}{\partial t} = \frac{\beta_{i,eff}}{\Lambda} \frac{f(z)}{A(z)} N(t) - \lambda_i C_i(z,t) - \frac{\partial}{\partial z} \frac{g(z,t) C_i(z,t)}{A(z)} \tag{2.3.6}$$

This model is the same as the neutronics model used in the EDF computational tool in the MOST study [4]. A difference is that in the EDF computational tool the fission shape $f(z)$ and adjoint flux shape $\varphi^{\dagger}(z)$ were computed in detail with another computational tool, where in our model only two shapes were investigated. Also in the EDF code two neutron energy groups were used, where in our model only one energy group is used.

2.4 Thermo hydraulic model

Thermal energy is generated inside the core through fission and transported out of the core by the circulating fuel-salt, from which heat is extracted in a heat exchanger outside the core. By far the greater part of the fission energy generated inside the core is deposited in the fuel-salt, but a small fraction (5% – 7.5%) is deposited within the graphite matrix. Since the fuel-salt is also the coolant in a MSR, the graphite temperature will be higher than that of the fuel-salt. But because the calculation of the graphite bulk temperature from the heat transfer between the graphite matrix and the fuel-salt is not a trivial job (see [4], p45-49), for simplicity it was assumed that the graphite temperature was the same as that of the fuel-salt.

The thermal hydraulic part of the model calculates the temperature of the fuel-salt as a function of z. In this model heat generation by fission, heat transport by forced convection due to the fuel-salt flow-rate, and cooling of the fuel-salt inside the heat exchanger are taken in consideration. Any other effects on the temperature of the fuel-salt are neglected.

The total amount of heat generated by fission inside the core (in Watt) is given by $P = N\mathrm{v}\Sigma_F p_{fiss}$. N is the total number of neutrons inside the core. v is their average velocity (in cm/s). Σ_F is the macroscopic fission cross section inside the core (in cm^{-1}) and is the probability a neutron will induce fission per cm traveled in the core. p_{fiss} is the average amount of energy generated per fission of a nucleus (in J/fission). To gain an expression for $\dot{q}'''(z)$, the heat generated per cm^3 as a function of z (in W/cm^3), P has to be multiplied by $f(z)/A(z)$. With the definition of $\Lambda \equiv (\mathrm{v}\nu\Sigma_F)^{-1}$ with ν the average number of neutrons generated per fission, $\dot{q}'''(z)$ can be written as:

$$\dot{q}'''(z,t) = \frac{p_{fiss}}{\Lambda\nu}\frac{f(z)}{A(z)}N(t) \tag{2.4.1}$$

Inside the heat exchanger, the fuel-salt is cooled according to Newton's Law

$$\phi_q = hOL\Delta T \tag{2.4.2}$$

where ϕ_q is the heat flow out of the fuel-salt (in W). h is the heat exchange coefficient of the heat exchanger (in W/cm^2K) (which depends on the fuel flow speed), L is the length of the heat exchanger (in cm), and O is the circumference of the heat exchanger (in cm). ΔT is the temperature difference (in K) between the fuel-salt $T(z,t)$ and the secondary cooling salt in the heat exchanger T_{he}. For simplicity the temperature T_{he} of the secondary coolant salt is assumed to be constant and a given parameter. The heat flow out of the fuel salt $\phi'''_{out}(z)$ (in W/cm^3), per cm^3 of fuel salt inside the heat exchanger as a function of z can be written as

$$\phi'''_{out}(z) = \frac{h(z)O(z)}{A(z)}\left(T(z,t) - T_{he}\right) \tag{2.4.3}$$

The convective term of the energy balance is given by $-\partial(uh_{fuel})/\partial z$ with $u(z,t)$ the flow speed of the fuel salt (in cm/s) and $h_{fuel}(z)$ the thermal energy of the fuel salt (in J/cm^3). With $u(z,t) = g(z,t)/A(z)$ and $h_{fuel}(z) = (\rho c_p)_f T(z,t)$ where ρ is the density of the fuel (in kg/cm^3) salt and c_p is its heat capacity (in J/kgK) this convective term becomes

$$\phi'''_{conv} = -\frac{\partial}{\partial z}\frac{g(z,t)}{A(z)}\left(\rho c_p\right)_f T(z,t) \tag{2.4.4}$$

The left hand side of the heat balance would normally read $\partial(h_{fuel})/\partial t$. But since the graphite temperature is the same as that of the fuel salt, inside the core any change of the fuel temperature also changes the graphite temperature, and $T(z,t)$ is effectively the temperature of both the fuel salt and the graphite inside the core. To accommodate for this, on the left hand side of the heat balance, the thermal energy of the graphite is added to that of the fuel salt and we get $\partial(h_{total}(z))/\partial t$ with $h_{total}(z) = h_{fuel} + h_{graphite}(z)$ is the total thermal energy per cm^3 fuel salt at position z and $h_{graphite}(z) = c_{p\_gr}T(z,t)M_{gr}/V_{fuel\_core}$ is the thermal energy of the graphite *per cm^3 fuel* at position z. Here M_{gr} is the total graphite mass inside the core (in kg), V_{fuel_core} is the total fuel volume inside the core (in cm^3) and a homogeneous distribution of both inside the core is assumed. c_{p_gr} is the heat capacity of the graphite (in J/kgK). With $h_{fuel} = (\rho c_p)_f T(z,t)$, h_{total} can be written as $h_{total} = (\rho c_p)_t(z)T(z,t)$ where $(\rho c_p)_t(z)$

$$\left(\rho c_p\right)_t(z) = \begin{cases} \text{Inside the core:} \quad \left(\rho c_p\right)_f + c_{p\_gr}M_{gr}/V_{fuel\_core} \\ \text{Outside the core:} \quad \left(\rho c_p\right)_f \end{cases} \tag{2.4.5}$$

is the energy needed to raise the temperature of the fuel salt at location z by one Kelvin, per cm^3 fuel salt.

Now the temperature of the fuel-salt at position z and time t $T(z,t)$ can be written as

$$\frac{\partial}{\partial t}\left(\rho c_p\right)_t(z)T(z,t) = \frac{p_{fiss}}{\Lambda \nu}\frac{f(z)}{A(z)}N(t) - \frac{\partial}{\partial z}\frac{g(z,t)}{A(z)}\left(\rho c_p\right)_f T(z,t) - \frac{h(z)O(z)}{A(z)}\left(T(z,t) - T_{he}\right) \tag{2.4.6}$$

which is the equation used to calculate the fuel salt temperature in our model.

2.5 Temperature feedback on reactivity

The reactivity ρ can change due to feedback from different factors. This can be from temperature changes, due to Doppler broadening and density changes, from pressure changes, gas bubbles developing in the fuel and many more things. The only feedback mechanism taken in consideration is the reactivity change due to a change in temperature.

The reactivity ρ of the reactor core depends on the temperature T of the fuel-salt and on that of the graphite. Since the temperature changes with time, so will the reactivity. The reactivity is zero at a certain equilibrium temperature T_0 (at which the reactor core is critical) and its temperature differential is α, which is called the temperature feedback coefficient on reactivity:

$$\frac{\partial \rho}{\partial T} = \alpha \tag{2.5.1}$$

from which follows the following equation for ρ.

$$\rho = \alpha(\langle T \rangle - T_0) \tag{2.5.2}$$

Here $\langle T \rangle$ is the weighted average temperature of the reactor core, where the temperature $T(z,t)$ of the reactor core is weighted with the fission shape $f(z)$. After all, $f(z)$ tells us how much a location contributes to the total fission inside the core, and a change in the temperature at a location where there is a lot of fission will have a stronger impact on the reactivity than a temperature change at a location where there is almost no fission. Or, in other words, a change in the capture, fission and absorption cross probabilities (the cross sections) at a location with a high neutron flux will have a stronger impact on the amount of neutrons that are created (and thus the reactivity) than that same change at a location where the neutron flux is low. The function for the reactivity ρ now becomes:

$$\rho(T) = \alpha\left(\int_0^H f(z)T(z,t)dz - T_0\right) \tag{2.5.3}$$

3 Implementation in computer code

To implement the formulas from the previous chapter in the computer code, they had to be discretized in both time and space. For the spatial discretization a finite volume method with an upwind model was used. Time was discretized using an implicit method.

For the discretization in space the whole fuel-salt flow loop of the MSR (core, pipes and heat exchanger) was divided in volume elements with a uniform length in the z direction of Δz and a volume of $A_j\Delta z$, where A_j is the cross-sectional area of element j through which the salt flows, perpendicular to the z-axis. This created $nelm = (H_{core} + L_{pipe1} + L_{he} + L_{pipe2}) / \Delta z$ elements. H_{core} is the height (in cm) of the core, L_{pipe1} and L_{pipe2} are the lengths of the pipes connecting the top of the core with the heat exchanger and the heat exchanger with the bottom of the core and L_{he} is the length of the heat exchanger (see figure 2.5). For those variables depending on z ($C_i(z,t)$, $T(z,t)$, etc.) this meant their value in the middle of each volume element was calculated. For those variables which functions where known beforehand ($f(z)$, $\varphi^*(z)$, etc.) their value in each element was calculated by integration over z over that volume element. Using an upwind model meant that when any convective term was discretized the value in the center of the 'downstream' volume cell of the transported variable was used as its value at the border of two cells.

Implicit time discretization means that for the calculation of every time derivative the values of the derived variable at the 'new time' (n+1) is used in the right hand side of the equation.

The equations for N and $C_i(z,t)$ were uncoupled and solved one after the other, because otherwise the matrix used to solve the set of linear equations would become very large. Every volume element of all 6 precursor groups would be needed, so the matrix would be 1 + 6$nelm$ by 1 + 6$nelm$, with $nelm$ the total number of volume elements. This way the precursor concentrations could be solved one group after another.

Since the various equations are uncoupled (to speed up calculation time), the various variables of interest are calculated one after the other and it depends on the order of the calculation in the computer code whether the 'old' value at time step n or the 'new' value at time step n+1 of a certain variable is used. In all discretized equations and in the flowchart in figure 3.1 these newest available values of a variable have a ^{n*}superscript, since they can be both the variable at time step n or n+1.

An extra iteration loop was included in the code to compensate for the uncoupling of the equations (the loop started by 'do until iter = number of iterations in figure 3.5). This extra iteration loop was never used though, since one pass was always enough to get results with the desired precision.

Initiate variables

Do till t = tmax

> $Nold = N^n$
>
> $C_i old = C_i^n$
>
> $Told = T^n$
>
> Do till iter = number of iterations
>
> > Set $g^{n+1}(t)$
> >
> > Calculate T^{n^*} $(g^{n^*}, N^{n^*}, T_{old})$
> >
> > Calculate ρ^{n^*} (T^{n^*})
> >
> > For all i
> >
> > > Calculate $C_{i,j}^{n^*}$ $(g^{n^*}, N^{n^*}, Cold)$
> >
> > Calculate $\rho_{rod}^{n^*}$ $(Nold, C_i^{n^*})$
> >
> > Calculate N^{n^*} $(C_i^{n^*}, \rho_{rod}^{n^*}, \rho^{n^*}, Nold)$
>
> $T^{n+1} = T^{n^*}$
>
> $\rho^{n+1} = \rho^{n^*}$
>
> $C_i^{n+1} = C^{n^*}$
>
> $\rho_{rod}^{n+1} = \rho_{rod}^{n^*}$
>
> $N^{n+1} = N^{n^*}$
>
> Write to file

Write to file

Figure 3.1: The flowchart of the computational model

3.1 Discretization of the fission shape and adjoint flux

The values of the functions $f(z)$ and $\varphi^{\dagger}(z)$ in each volume element j could be evaluated analytically from (2.3.1), (2.3.2), (2.3.3) and (2.3.4) by integrating over the volume element j. This gives

$$f_j = \int_{(j-1)\Delta z}^{j\Delta z} \sin\left(\pi\left(z + \tfrac{1}{2}\lambda_{extrap}\right)/H_{ex}\right)dz \,/ \int_0^H \sin\left(\pi\left(z + \tfrac{1}{2}\lambda_{extrap}\right)/H_{ex}\right)dz \qquad (3.1.1)$$

$$\varphi_j^{\dagger} = \int_{(j-1)\Delta z}^{j\Delta z} \sin\left(\pi\left(z + \tfrac{1}{2}\lambda_{extrap}\right)/H_{ex}\right)dz \qquad (3.1.2)$$

inside the reactor core, and $f_j = \varphi_j^{\dagger} = 0$ outside the core ($z > H$) for the case of a sine shaped fission shape and adjoint flux.

In the case $f(z)$ and $\varphi^{\dagger}(z)$ were taken flat, their discretized values inside the reactor core became:

$$f_j = \Delta z / H_{core} = 1 / ncore \tag{3.1.3}$$

$$\varphi_j^{\dagger} = 1 \tag{3.1.4}$$

where *ncore* is the number of elements in which the reactor core was divided. Please note that by calculating the values for f_j and $\varphi_j^{\dagger}$, they don't actually represent the average value (or the central value) of the functions $f(z)$ and $\varphi^{\dagger}(z)$ in volume element j, but their average value multiplied by Δz. It can also be said they represent the integral of the functions over the volume element j. This was a slight mistake corrected by dividing the values of f_j and $\varphi_j^{\dagger}$ when necessary by Δz in the other discretized functions.

3.2 Numerical solution of the number of neutrons

The discretized version in time and space of equation (2.3.5) for the number of neutrons N in the reactor core, with implicit time discretization is:

$$\frac{N^{n+1} - N^n}{\Delta t} = \frac{\rho^{n*} + \rho_{rod}^{n*} - \beta_{eff}}{\Lambda} N^{n+1} + \sum_{i=1}^{6} \lambda_i \frac{\sum_j A_j \Delta z C_{i,j}^{n*} \varphi_j^{\dagger}}{\sum_j f_j \varphi_j^{\dagger}} \tag{3.2.1}$$

with N^{n+1} the number of neutrons at time $t = \Delta t \cdot (n+1)$ and N^n the number of neutrons in the previous time step. $\Delta\rho^{n*}$, ρ_{rod}^{n*} and $C_{i,j}^{n*}$ are the newest available values for the reactivity and the precursor concentrations. The Δz term in the upper sum in the right hand term comes from the integration over z. This term is not included in the lower sum of $f_j \varphi_j^{\dagger}$, since Δz is already included in f_j.

Solving (3.2.1) for N^{n+1} is straightforward, since it is uncoupled from the precursor equations.

$$N^{n+1} = \left(\frac{N^n}{\Delta t} + \sum_{i=1}^{6} \lambda_i \frac{\sum_j A_j \Delta z C_{i,j}^{n*} \varphi_j^{\dagger}}{\sum_j f_j \varphi_j^{\dagger}} \right) \left(\frac{1}{\Delta t} - \frac{\rho^{n*} + \rho_{rod}^{n*} - \beta_{eff}}{\Lambda} \right)^{-1} \tag{3.2.2}$$

This is the expression for the number of neutrons at time $t = \Delta t \cdot (n+1)$ as implemented in the computer code.

3.3 Numerical solution of the precursor concentration

Discretizing (2.3.6) by dividing space in portions of Δz and using the precursor concentration in volume cell j as the precursor concentration in the fuel flowing out of cell j (upwind model) gives:

$$\frac{dC_{i,j}(t)}{dt} = \frac{\beta_{i,eff}}{\Lambda}\frac{f_j}{\Delta z A_j}N(t) - \lambda_i C_{i,j}(t) - \frac{g(t)C_{i,j}(t)}{A_j \Delta z} + \frac{g(t)C_{i,j-1}(t)}{A_j \Delta z} \tag{3.3.1}$$

Here the fact that $g(t)$ is not a function of z and $A(z)$ is constant in each volume cell is used. f_j is divided by Δz to gain the correct value. Implicit time discretization of (3.3.1) now gives:

$$\frac{C_{i,j}^{n+1} - C_{i,j}^{n}}{\Delta t} = \frac{\beta_{i,eff}}{\Lambda}\frac{f_j N^{n^*}}{A_j \Delta z} - \lambda_i C_{i,j}^{n+1} - \frac{g^{n^*}C_{i,j}^{n+1}}{A_j \Delta z} + \frac{g^{n^*}C_{i,j-1}^{n+1}}{A_j \Delta z} \tag{3.3.2}$$

where the terms with $^{n^*}$ superscript represent the newest available values for those terms. $C_{i,j}^{n}$ is the value of the precursor concentration of precursor group i in unit cell j at time $t = \Delta t \cdot n$ and $C_{i,j}^{n+1}$ at time $t = \Delta t \cdot (n+1)$.

(3.3.2) can be written as a system of linear equations of $C_{i,j}^{n+1}$:

$$\left(\frac{1}{\Delta t} + \lambda_i + \frac{g^{n^*}}{A_j \Delta z}\right)C_{i,j}^{n+1} - \frac{g^{n^*}}{A_j \Delta z}C_{i,j-1}^{n+1} = \frac{\beta_{i,eff}}{\Lambda}\frac{f_j N^{n^*}}{A_j \Delta z} + \frac{C_{i,j}^{n}}{\Delta t} \tag{3.3.3}$$

for j is 1 to the number of elements, *nelm*. Since the fuel is pumped around we have a cyclic boundary condition of $C_{i,0} = C_{i,nelm}$. (3.3.3) can be written as a matrix-vector equation

$$\underline{\underline{A}}\,\underline{C}_i^{n+1} = \underline{B} \tag{3.3.4}$$

with matrix $\underline{\underline{A}}$ of the form:

$$\underline{\underline{A}} = \begin{bmatrix} a_1 & & & b_1 \\ b_2 & a_2 & & \\ & b_j & a_j & \\ & & b_n & a_n \end{bmatrix} \quad \begin{cases} a_j = \dfrac{1}{\Delta t} + \lambda_i + \dfrac{g^{n^*}}{A_j \Delta z} \\ b_j = -\dfrac{g^{n^*}}{A_j \Delta z} \end{cases} \tag{3.3.5}$$

and vector $\underline{B}$ as

$$\underline{B} = \frac{\beta_{i,eff}}{\Lambda} \frac{\underline{f} N^{n^*}}{\underline{A} \Delta z} + \frac{\underline{C}_i^n}{\Delta t} \tag{3.3.6}$$

In which $\underline{f}$, $\underline{A}$ and $\underline{C}_i^n$ are the vectors constructed from the f_j's, A_j's and $C_{i,j}^n$'s.

The matrix $\underline{\underline{A}}$ and vector $\underline{B}$ are constructed in the computer code. With a FORTRAN driver routine from LAPACK [6] the system in (3.3.4) is then solved numerically and the new values for the precursor concentrations $C_{i,j}^{n+1}$ are calculated.

3.4 Calculation of the temperature of the fuel-salt

Space discretization of (2.4.6) in units of Δz, and assuming the value of the temperature at a boundary of two unit cells is the value in the cell the flow is coming from (upwind model), gives

$$\begin{aligned} \left(\rho c_p\right)_{t,j} \frac{\partial T_j(t)}{\partial t} = \frac{p_{fiss}}{\Lambda \nu} \frac{f_j}{A_j \Delta z} N(t) - \frac{g(t)\left(\rho c_p\right)_f T_j(t)}{A_j \Delta z} + \frac{g(t)\left(\rho c_p\right)_f T_{j-1}(t)}{A_j \Delta z} \\ - \frac{h_j O_j}{A_j \Delta z} T_j(t) + \frac{h_j O_j}{A_j \Delta z} T_{he} \end{aligned} \tag{3.4.1}$$

To see that it is correct that in the contribution of the temperature change by flow the volume of cell j ($A_j \Delta z$) is used in both the inflow as well as the outflow by multiplying the whole equation by this term. The equation then becomes: the change in energy of volume cell j (in J/s) is the generation, minus outflow plus inflow due to fuel flow, minus outflow plus inflow due to cooling.

Implicit time discretization of (3.4.1) and dividing both sides by $(\rho c_p)_{t,j}$ gives

$$\begin{aligned} \frac{T_j^{n+1} - T_j^n}{\Delta t} = \frac{p_{fiss}}{\Lambda \nu} \frac{f_j}{\left(\rho c_p\right)_{t,j} A_j \Delta z} N^{n^*} - \frac{\left(\rho c_p\right)_f g^{n^*} T_j^{n+1}}{\left(\rho c_p\right)_{t,j} A_j \Delta z} + \frac{\left(\rho c_p\right)_f g^{n^*} T_{j-1}^{n+1}}{\left(\rho c_p\right)_{t,j} A_j \Delta z} \\ - \frac{h_j O_j}{\left(\rho c_p\right)_{t,j} A_j \Delta z} T_j^{n+1} + \frac{h_j O_j}{\left(\rho c_p\right)_{t,j} A_j \Delta z} T_{he} \end{aligned} \tag{3.4.2}$$

where again a variable with the $^{n^*}$ superscript denotes the newest available value of that variable. T^{n+1} is the temperature of the fuel-salt at time $t = \Delta t \cdot (n+1)$, and T^n is the old temperature of the fuel-salt.

Equation (3.4.2) can also be written as a system of linear equations of T_j^{n+1} for j = 1 to *nelm*:

$$T_j^{n+1}\left(\frac{1}{\Delta t}+\frac{\left(\rho c_p\right)_f g^{n*}}{\left(\rho c_p\right)_{t,j} A_j\Delta z}+\frac{h_j O_j}{\left(\rho c_p\right)_{t,j} A_j\Delta z}\right)-T_{j-1}^{n+1}\frac{\left(\rho c_p\right)_f g^{n*}}{\left(\rho c_p\right)_{t,j} A_j\Delta z}=$$
$$\frac{p_{fiss}}{\Lambda\nu}\frac{f_j}{\left(\rho c_p\right)_{t,j} A_j\Delta z}N^{n*}+\frac{h_j O_j}{\left(\rho c_p\right)_{t,j} A_j\Delta z}T_{he}+\frac{T_j^n}{\Delta t} \tag{3.4.3}$$

or

$$\underline{\underline{A}}\,\underline{T}^{n+1}=\underline{B} \tag{3.4.4}$$

with matrix $\underline{\underline{A}}$ of the form:

$$\underline{\underline{A}}=\begin{bmatrix} a_1 & & & b_1 \\ b_2 & a_2 & & \\ & b_j & a_j & \\ & & b_n & a_n \end{bmatrix} \quad \begin{cases} a_j=\dfrac{1}{\Delta t}+\dfrac{\left(\rho c_p\right)_f g^{n*}}{\left(\rho c_p\right)_{t,j} A_j\Delta z}+\dfrac{h_j O_j}{\left(\rho c_p\right)_{t,j} A_j\Delta z} \\ b_j=-\dfrac{\left(\rho c_p\right)_f g^{n*}}{\left(\rho c_p\right)_{t,j} A_j\Delta z} \end{cases} \tag{3.4.5}$$

and vector $\underline{B}$ is

$$\underline{B}=\frac{p_{fiss}}{\Lambda\nu}\frac{N^{n*}}{\Delta z}\frac{\underline{f}}{\underline{\left(\rho c_p\right)_t}\,\underline{A}}+\frac{T_{he}}{\Delta z}\frac{\underline{hO}}{\underline{\left(\rho c_p\right)_t}\,\underline{A}}+\frac{1}{\Delta t}\underline{T}^n \tag{3.4.6}$$

In which $\underline{f}$, $\underline{A}, \underline{C}_i^n$ and $\underline{\left(\rho c_p\right)_t}$ are, as before, the vectors constructed from the f_j's, A_j's, $C_{i,j}^n$'s and $\left(\rho c_p\right)_{t,j}$'s.

Matrix $\underline{\underline{A}}$ and vector $\underline{B}$ are again constructed in the computer code from the old values of the various variables, after which the system in (3.4.4) is solved numerically with a driver routine from LAPACK [6].

3.5 Calculation of the reactivity

Space discretization of (2.5.3) gives:

$$\rho^{n+1}=\alpha\left(\sum_j\left(f_j T_j^{n*}\right)-T_0\right) \tag{3.5.1}$$

where the fact that the value f_j is already an integral over Δz was used. ρ^{n+1} is the reactivity change due to temperature feedback at time $t = \Delta t{\cdot}(n{+}1)$ and $T_j^{n^*}$ is the newest available temperature of the fuel-salt in volume cell j. The sums are over the volume elements of the core only, since outside the core f_j is zero and there is no fission.

4 Benchmarks

At the MSRE several experiments were conducted that are well suited to use as benchmarks for the developed computational tool. These include several zero-power experiments, both at steady state and dynamic, and one low power natural convection transient.

In a zero-power experiment there is no power generated in the reactor, so the temperature does not change and there will be no temperature feedback on the reactivity. For the computational tool it means the parts where the reactivity and temperature are calculated are simply skipped and $\rho(T)$ was set to zero.

To find steady state solutions, calculations were run for a large total time t_{max}. This t_{max} was chosen sufficiently big that no changes in any of the calculated variables were observed for at least the last 300 s of simulated time. These variables were all plotted with at least 5 significant numbers. For the calculations of the steady state solutions usually a larger time step Δt was used than in the calculation of the transients, where the time scale was of importance. It was noticed that with steady state calculations the final solution would be the same for large and small Δt, although the simulated time t_{max} at which steady state was reached might not be. But in transient calculations the results would be different if Δt was taken too large.

All numerical values of the different variables used in the calculations, such as geometric data of the MSR, fuel salt density, and the β_{eff} of the various fuels used can be found in Appendix B: MSR data.

4.1 Benchmark 1: Reactivity lost due to fuel motion

4.1.1 Explanation of the benchmark

When the fuel flow is zero and the core is critical, a certain steady state solution of the neutron density and precursor concentrations inside the core is formed. There will be no precursors outside the core. When the pump is now turned on and the fuel starts flowing, precursors flow out of the reactor core and those neutrons that are emitted when the precursors decay outside the core are lost for the fission process, causing a loss of reactivity inside the core. To keep the core critical, this loss has to be compensated by inserting the same amount of reactivity in the core (by extracting a control rod for example). After some time a new steady state will be formed in which the precursors are pumped around at a certain speed and a set percentage decays outside the reactor core. The reactivity that needs to be added to keep the core critical in this steady state situation, compared to the situation with no fuel flow, is the reactivity lost, β_{lost}, due to the fuel motion.

Two types of fuel were used in the MSRE, Uranium-235 fuel and Uranium-233 fuel, each with different values for Λ, v, β_i and λ_i. For both of these fuels the reactivity lost due to fuel motion, β_{lost}, was measured for nominal fuel-salt flow-rate, $g = 80.247*10^3$ cm^3/s, the flow-rate at which the MSR in the MSRE ran during normal operation. Additionally, the β_{lost} was also calculated numerically at the ORNL. In the MOST project [3], for each of these two fuels β_{lost} was calculated using two sets of precursor decay data. The first set is the ORNL precursor decay data, measured by the ORNL at the MSRE (table 8.3). The second set is a set of precursor decay data calculated from the JEF database (table 8.4). Our results will be compared with both the measured β_{lost} at the MSRE, and the β_{lost} calculated at the ORNL and by the EDF code in the MOST project.

To make sure only the effect of the fuel motion on the reactivity was calculated, this benchmark was run at zero power. For this benchmark, first the steady state solution for a critical core with zero fuel flow was calculated, when β_{lost} = 0 of course. To find the steady state solution with no fuel flow, the fuel-salt flow-rate g was set to zero. The initial value of the number of neutrons N was set to 10^9 and for the precursor concentrations $C_{i,j}$ the analytical solution of

$$C_{i,j}(0) = \frac{\beta_{i,eff}}{\Lambda\lambda_i}\frac{f_j N(0)}{\Delta z A_j} \text{ for all } j \text{ inside the core, 0 outside the core.} \qquad (4.1.1)$$

was used. This analytical solution was found by solving (3.3.1) for $C_{i,j}$, with $dC_{i,j}/dt = 0$ (steady state). As a check of our computational model, the time step Δt was set to 0.1 s and the simulation was run for 1000 s. In none of the cases did the precursor concentrations or the number of neutrons change during this time. This is a nice conformation that the basic neutronics model was indeed implemented correctly. See also section 9.1 in appendix C for a plot of the analytical solution and one calculated with the computational tool (figure 9.1).

The neutron and precursor concentration data from the steady state solution was then used as input for the evaluation of β_{lost} due to fuel flow. At t = 0 the fuel flow g was set at the nominal flow rate of 80.247*10^3 cm^3/s, after which the precursor concentrations in the primary loop were calculated every time step. With the precursor concentrations known, β_{lost} was calculated by replacing ρ_{rod} with β_{lost} in (3.2.1) and setting $dN/dt = 0$ ($N^{n+1} = N^n$). Solving for β_{lost} gives the following equation

$$\beta_{lost} = \beta_{eff} - \frac{\Lambda}{N^n}\sum_{i=1}^{6}\lambda_i \frac{\sum_j A_j \Delta z C_{i,j}^{n*}\varphi_j^\dagger}{\sum_j f_j \varphi_j^\dagger} \qquad (4.1.2)$$

The program was run until the system was again in (a new) steady state.

The EDF model evaluated in the MOST study calculated the shapes of the adjoint flux $\varphi^\dagger(z)$ and the fission shape $f(z)$ were calculated in detail. In the current model however, for simplicity only two different shapes were considered for the adjoint flux and fission shape, the sine-shape and the flat shape. An important part of this benchmark was evaluating which shape of the adjoint flux and the fission shape gave the best results with our computational tool and should be used in the rest of the benchmarks.

4.1.2 Results and discussion

The simulation was run with a time step Δt = 0.1 s and for a total time of 1000 s. For all calculations no changes in the values of β_{lost} or $C_{i,j}$ was observed after 500 seconds of simulated time had passed, so the 1000 s was more than sufficient time to attain steady state. The β_{lost} data for nominal fuel flow-rate, $g = 80.247*10^3$ cm^3/s, is given in the table below for the various precursor decay data, adjoint flux shapes and fuels used. No calculations were performed with a flat shaped fission shape and sine shaped adjoint flux shape, since the other calculations already showed these shapes gave worse results than their counterparts.

Table 4.1: β_{lost} (in pcm) due to fuel motion for the two different fuels and precursor decay data sets, as calculated with the developed code for different adjoint flux shapes, as well as calculated by different computer codes and as measured in the MSRE.

	U-235 ORNL	U-235 JEF	U-233 ORNL	U-233 JEF
MSRE [4]	212	-	100 ±5	-
ORNL Calc. [4]	222	-	100.5	-
EDF [4]	228.8	207.6	107.8	101.4
Flat $\varphi^*(z)$, sine $f(z)$	237.294	232.911	118.278	121.453
Flat $\varphi^*(z)$ and $f(z)$	253.281	251.7	123.890	128.679
Sine $\varphi^*(z)$ and $f(z)$	279.6	275.837	137.526	142.161

The results from the calculations of β_{lost} using a sine shaped fission shape and a flat adjoint flux (See (3.1.1) and (3.1.3)) gave results in better agreement with the experimental data from the MSRE than those with both a sine shaped adjoint flux and fission shape, or with both a flat adjoint flux and fission shape. The fact that a flat adjoint flux shape gave good results suggests that the location inside the core at which neutrons are emitted by the precursors has little effect on their worth for the fission process. A delayed neutron emitted near the edge of the core has the same value for the fission process as those emitted in the center of the core. A flat adjoint flux shape gives a lower β_{lost} than a sine shaped $\varphi^\dagger(z)$, since with a flat $\varphi^\dagger(z)$ the shift of the high concentration of precursors created at the center of the core towards the edge due to fuel motion has no effect on the amount of neutrons created. A sine shaped fission shape gives a lower β_{lost} than a flat $f(z)$, since with a sine shape most precursors will be created at the center of the core and fewer near the edge of the core than with a flat $f(z)$. Thus fewer precursors will be moved out of the core by the fuel flow. For all further calculations, a flat adjoint flux and a sine shaped fission shape were used.

The values of β_{lost} calculated with a flat adjoint flux and a sine shaped fission shape were about 10% bigger than the experimental results for U-235 fuel and 20% for U-233 fuel. There are three major simplifications in the computational model that affect the calculated β_{lost}. The fuel flow model is modeled as a plug flow everywhere, with a uniform flow speed and no mixing in the pump or plenums. The second important simplification is in the used adjoint flux and fission shapes. Finally, it was assumed there was no radial dependence on any variable.

The result of the first simplification is basically to reduce (cancel) any mixing of the fuel salt, except due to numerical diffusion (see section 9.3, figure 9.2). From [7] it was noticed that mixing of the fuel actually causes a higher β_{lost}. So the simplifications in the fuel flow probably don't cause a higher calculated β_{lost} than measured in the MSRE.

When comparing the calculated β_{lost} for the different adjoint flux and fission shapes, it was noticed that these shapes can have a large affect on the value of β_{lost}. The fact that only two simple shapes were considered for $\varphi^{\dagger}(z)$ and $f(z)$, instead of a detailed calculation as was done in the EDF code, will influence the calculated β_{lost}.

The third simplification used in the model, that all variables could be approximated by functions of z only, may have the largest effect on the calculated β_{lost}. It was assumed that the shapes of $\varphi^{\dagger}$ and f were uniform in the r direction throughout the whole core height, and that the flow speed was uniform with r. In reality this is very unlikely.

Still, the calculated values were comparable with results from other computer codes and the measurements in the MSRE, and it can be concluded that the developed model is capable of finding reliable steady state solution in the zero-power regime for the molten salt reactor.

β_{lost} versus fuel flow speed

For U-235 and U-233 fuel with ORNL and JEF precursor decay data, with a flat adjoint flux and a sine shaped fission shape, β_{lost} was evaluated for different fuel-salt flow-rates and a graph of β_{lost} versus the flow-rate g was made (figure 4.1). For a table with the calculated values, see table 7.1. The time step Δt used in the calculation of the steady state was set to 1 second after tests showed that β_{lost} still converged to the same value as for smaller time steps (0.1 and 0.01 s).

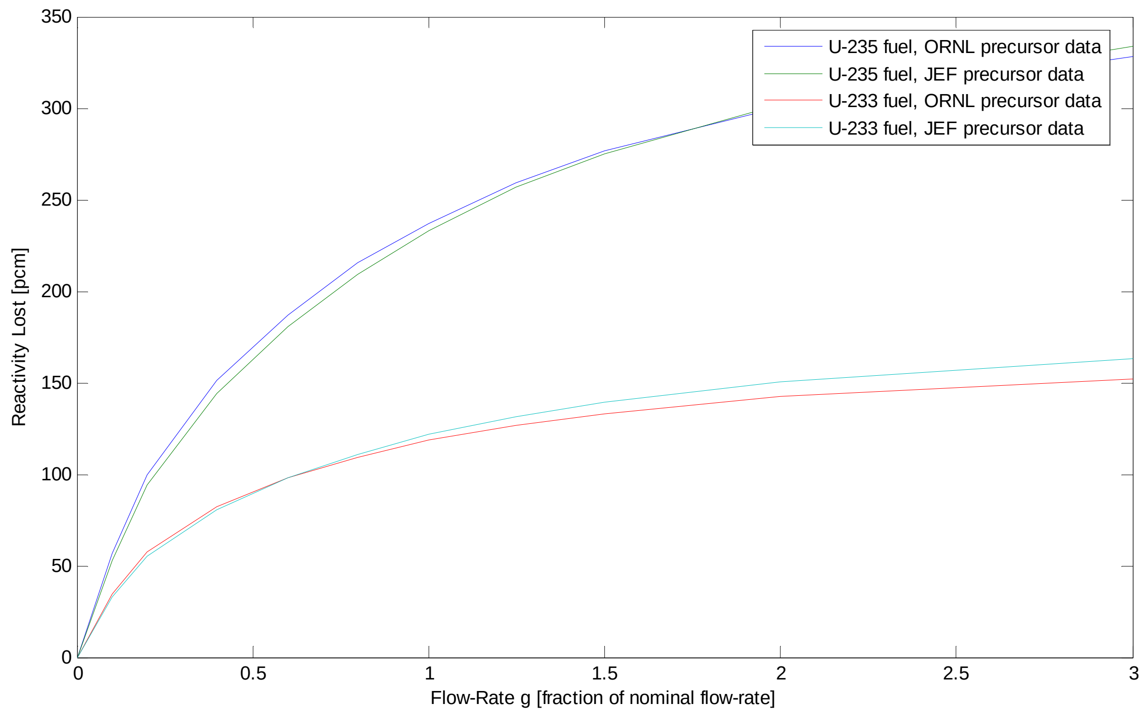

Figure 4.1: β_{lost} in pcm versus the flow-rate g (as a fraction of $g_{nom} = 80.247*10^3$ cm^3/s) for the two different fuels and the two different precursor decay data sets.

When compared to another study on the reactivity lost versus fuel flow [7], the shape of β_{lost} as a function of the flow-rate g is in agreement with these results. Unfortunately, no numerical data from other measurements or calculations were available to compare the β_{lost} with at fuel flow-rates other than the nominal flow-rate during the MSRE. The asymptotic behavior of the graph of β_{lost} is as expected. As the fuel flow rises, more precursors generated inside the core are swept out of the core, but also a higher percentage of the precursors swept outside the core will flow back inside at the other end of the loop, before they had time to decay. This compensates in part for those extra precursors leaving the core. As the flow rate rises further, the precursor concentration will become more and more uniform throughout the whole flow loop and at infinite flow rate the precursor concentration will be the same everywhere in the primary loop. This asymptotic value of β_{lost} can be calculated with (2.3.6). Use the fact that $C_i(z,t)$ is constant over z, set the time derivative to zero since we are looking for a steady state solution, and integrate over the whole primary flow loop. The convective term will disappear since we use a circular integral. This gives the following equation for C_i at infinite flow speed g_{inf}:

$$\lambda_i C_i V_{loop} = \frac{\beta_{i,eff} N}{\Lambda} \rightarrow C_i = \frac{\beta_{i,eff} N}{\Lambda \lambda_i V_{loop}} \qquad (4.1.3)$$

With V_{loop} the total fuel volume in the primary loop (in cm^3). Filling in this result in (2.3.5) (use C and A constant in core, steady state so time derivative is zero, rhorod = betalost, rho(T) = 0)

$$0 = \frac{\beta_{lost} - \beta_{eff}}{\Lambda} N(t) + \sum_{i=1}^{6} \frac{\beta_{i,eff} N}{\Lambda} \frac{A_{core}}{V_{loop}} \frac{\int_0^H \varphi^\dagger(z)dz}{\int_0^H f(z)\varphi^\dagger(z)dz}$$

$$\beta_{lost} = \beta_{eff} \left(1 - \frac{A_{core}}{V_{loop}} \frac{\int_0^H \varphi^\dagger(z)dz}{\int_0^H f(z)\varphi^\dagger(z)dz} \right) \tag{4.1.4}$$

with adjoint flux = 1 and integral over f(z) = 1 we get:

$$\beta_{lost} = \beta_{eff} \left(1 - \frac{A_{core}}{V_{loop}} H_{core} \right) = \beta_{eff} \left(1 - \frac{V_{core}}{V_{loop}} \right) \tag{4.1.5}$$

With $V_{core} = 0.8188*10^6$ cm^3 and $V_{loop} = 2.0208*10^3$ cm^3, $V_{core}/V_{loop} = 0.4052$ and the asymptotic values for β_{lost} are given in table 4.2. The values are in agreement with the plots in figure 4.1.

Table 4.2: Analytical solution of β_{lost} values in pcm for infinite flow-rate g_{inf}.

	U-235, ORNL	U-235, JEF	U-233, ORNL	U-233, JEF
β_{lost} at g_{inf}	396.2	437.9	172.1	194.1

4.2 Benchmark 2: Fuel-pump start-up transient

4.2.1 Explanation of the benchmark

In this benchmark the transient of the reactivity lost due to fuel motion during the first 50 seconds after the fuel-pump is turned on is calculated. The benchmark is again performed at zero-power operating conditions, so there will be no temperature feedback on the reactivity. Initially the fuel is stationary (g = 0 cm^3/s) and the core is critical, which are the same initial conditions as in the previous benchmark. The fuel pump is turned on at t = 0. This causes the fuel-salt flow speed to rise in time towards its nominal flow speed (g_{nom} = 80.247*10^3 cm^3/s). As explained before, pumping the fuel around causes a loss of reactivity as precursors are swept outside the core. Reactivity will have to be added (by withdrawing a control rod) to keep the power at a constant level. The reactivity that needs to be added as a function of time is calculated and compared to the measurements done in the MSRE, and calculations done by the EDF computer code in the MOST study.

The formula to calculated the reactivity that needs to be inserted in the reactor core to return the power to its initial value at t = 0 can be derived from (3.2.1). The power generated in the reactor core at time $t = \Delta t(n+1)$ is the same as that at t = 0 if the number of neutrons in the reactor core at that time, N^{n+1}, is equal to the initial number of neutrons in the reactor core at t = 0, N^0. Insert $N^{n+1} = N^0$ in (3.2.1), $\rho^{n^*} = 0$ since it is a zero-power benchmark, and solve the equation for ρ_{rod} to get

$$\rho_{rod}^{n+1} = \frac{\Lambda}{\Delta t} - \frac{\Lambda}{N^0}\left(\frac{N^n}{\Delta t} + \sum_{i=1}^{6}\lambda_i \frac{\sum_j A_j \Delta z C_{i,j}^{n*}\varphi_j^\dagger}{\sum_j f_j \varphi_j^\dagger}\right) + \beta_{eff} \tag{4.2.1}$$

which is the reactivity that has to be inserted, $\rho_{inserted}$, to keep the number of neutrons (and thus the power) at its initial value of N^0.

In the reactor used in the MSRE the maximum rate of reactivity insertion, because of the limitation on the movement speed of the control rod, was limited to 29.41 pcm/s. The fuel-pump start-up transients were calculated both with and without this limitation. The transient was calculated for U-235 fuel using both the ORNL (fig 4.2) and JEF (fig 4.3) precursor decay data (see Appendix B for the data).

There is no data available of the fuel-salt flow-rate versus time, $g(t)$, during the fuel-pump start-up transient in the MSRE. The fuel-salt flow-rate start-up characteristic had to be derived from a figure with the start-up characteristics for fuel- and coolant-pump speeds and for coolant-salt flow rates [3, figure 2.10]. In [8] a model for the flow-rate at start-up of $g(t) = g_{nom}(1 - e^{-t/\tau})$ was suggested. This certainly could be used to model part of the flow-rate during start-up, but during the first few seconds of the transient $g(t)$ had a distinctly different behavior. This was modeled by $g(t) = g_{nom}(e^{t \cdot \tau 2} - 1)$. The following formula for the fuel flow $g(t)$ during pump start-up was used:

$$g(t) = \begin{cases} g_{nom} \cdot (e^{t \cdot 0.5993} - 1) & t < 0.5625 \\ g_{nom} \cdot (1 - e^{-(t-0.15625)/0.793}) & 0.5625 < t < 10 \\ g_{nom} & t > 10 \end{cases} \tag{4.2.2}$$

For further details on the estimation of the fuel-salt flow-speed $g(t)$ during fuel-pump start-up see appendix 7.2.

4.2.2 Results and discussion

The simulation was run with a time step Δt = 0.01 s and for 50 s.

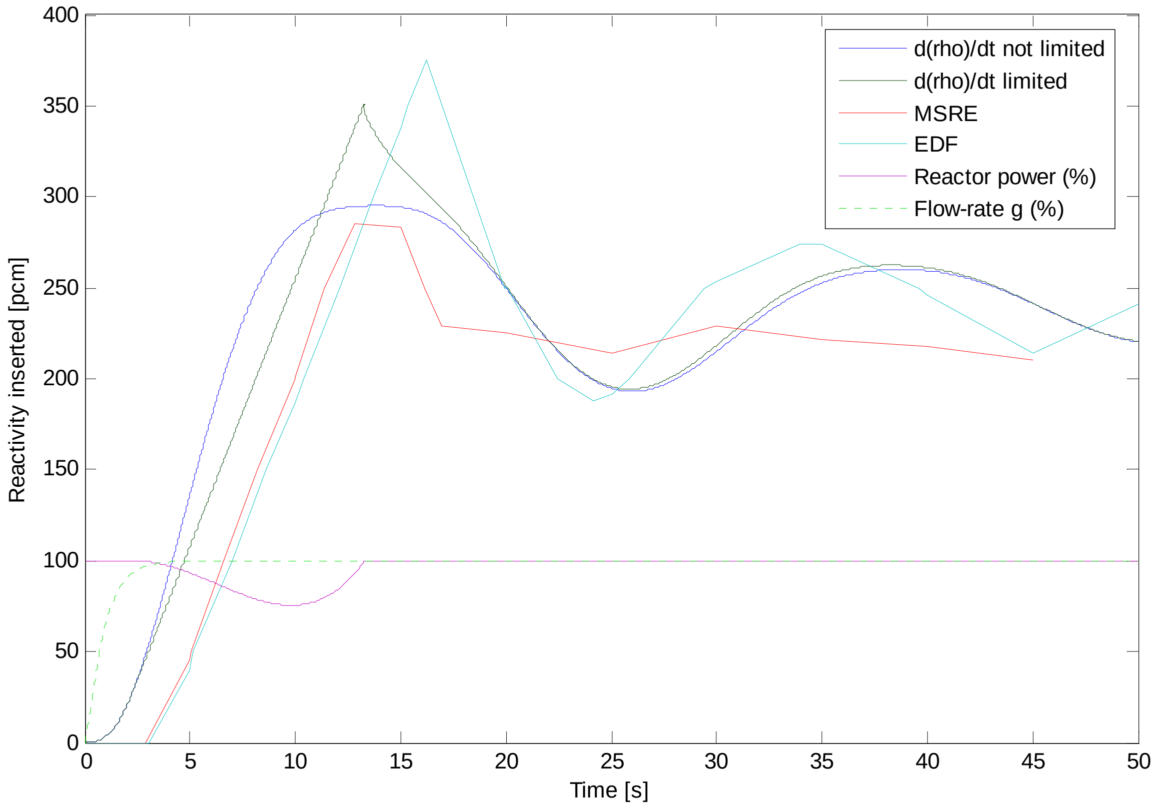

Figure 4.2: Reactivity inserted during fuel-pump start-up transient using ORNL precursor decay data. Calculated for the case the speed of reactivity change was restricted and not restricted, as calculated by the EDF code [4] and as measured in the MSRE. Also plotted is the flow-rate of the fuel-salt in percentage of nominal flow-rate (100% = $80.247 \cdot 10^3$ cm^3/s) and the reactor power in % of its initial value for the cause $d\rho_{rod}/dt$ was limited.

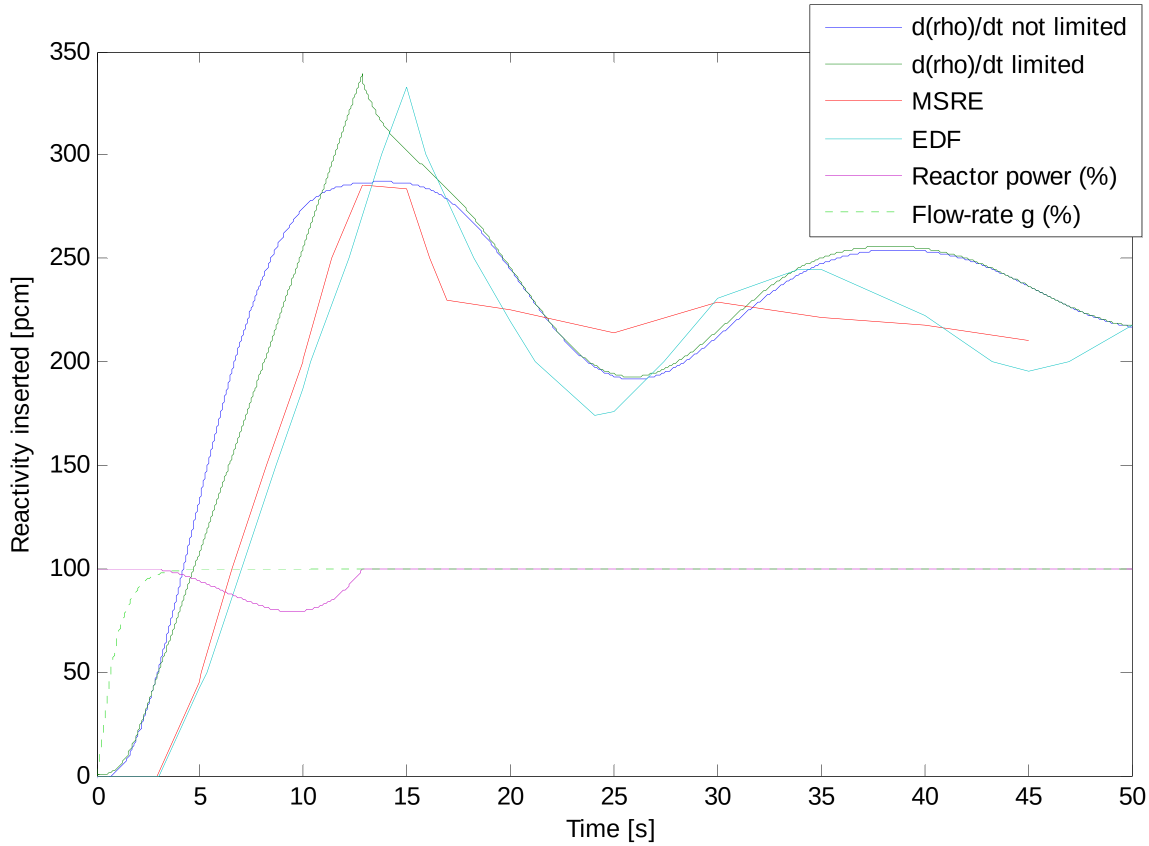

Figure 4.3: Reactivity inserted during fuel-pump start-up transient using JEF precursor decay data. Calculated for the case the speed of reactivity change was restricted and not restricted, as calculated by the EDF code [4] and as measured in the MSRE. Also plotted is the flow-rate of the fuel-salt in percentage of nominal flow-rate (100% = $80.247 \cdot 10^3$ cm^3/s) and the reactor power in % of its initial value for the cause $d\rho_{rod}/dt$ was limited.

The jagged plots of the reactivity inserted for the MSRE and the EDF code come from the fact that they are constructed from about twenty points each, which were evaluated manually from plots for these values printed out on paper. Unfortunately no tabular data was available.

The basic characteristic of the fuel-pump start-up transient of the MSRE was followed, which means an initial overshoot of $\rho_{inserted}$, after which it dampened down towards its steady state value of β_{lost} for nominal flow speed.

The maximum $\rho_{inserted}$ with no restriction on the speed of insertion of reactivity occurs right before precursors reenter the core, which is indeed after about 14 seconds (the time for fuel to travel from core outlet to inlet at nominal flow speed is almost 14 seconds). After this moment, those precursors that have not yet decayed start reentering the core, thus raising the reactivity (and less reactivity has to be inserted to keep the core critical). The extra overshoot in the case where the speed of insertion of reactivity was limited is caused by the fact that during the first part of the transient, reactivity cannot be inserted fast enough to keep the reactor at its initial power level, and the reactor power drops, as can be seen in the plots. To compensate for this, extra reactivity is inserted as soon as possible until the power is back to its initial value. In this case the peek value of $\rho_{inserted}$ actually occurs at the moment the reactor power is back at its initial value. As was mentioned in the MOST report [4], the power dropped to a minimum value of about 80% of its initial value before rising back. This is in accordance with the minimum power calculated by the computational model.

The results from MSRE and EDF lag the calculated values by almost two seconds. This is probably caused by a different choice of the flow-rate during pump start-up (with zero or very low values of $g(t)$ during the first two seconds of the transient).

The calculated overshoot of $\rho_{inserted}$ was higher than that measured in the MSRE (though it was of the same magnitude of the value calculated by EDF). This might be caused by a certain amount of mixing of the fuel in the MSRE. As noted before, in our computer model the flow-rate is the same everywhere and no mixing or diffusion occurs, except for numerical diffusion (see section 9.3, figure 9.2). In the real case this is highly improbable. Mixing, especially in the plenums, would cause a more even distribution of the precursors in the loop, thus causing some precursors to start reentering the core more quickly than expected, thus raising the reactivity inside the core and lowering the amount of reactivity that had to be inserted.

The strong oscillation of $\rho_{inserted}$ was not observed in the data from the MSRE. Oscillations were expected, because of the reentry of precursors after the fuel has circulated the primary loop. In the initial condition, there is a large peek of precursors inside the core, and there are no precursors outside the core. Every time this peek reenters the core, the reactivity would rise again, while every time the part where no precursors are present would enter the core, the reactivity would drop and more reactivity would have to be inserted to keep the core critical. As the distribution of the precursors in the fuel loop becomes more even and the initial large peek in precursor concentrations degrades, the oscillation of $\rho_{inserted}$ dampens out towards the steady state situation. As was expected, the period of the oscillation coincides with the circulation time of the fuel (about 25 seconds). Most calculation tools tested in [4] showed these same fluctuations. (Simmer, DYN1D-MSR, EDF). In the MSRE, as was noted above, mixing of the fuel was far more prominent. This would result in a more even distribution of precursor concentrations, quickly smearing out the initial peek of the precursors resulting from the stationary situation towards the areas in the loop where there were initially no precursors present, thus taking away the cause of the oscillations in $\rho_{inserted}$.

The only difference between the results using ORNL and JEF precursor decay data is the height of $\rho_{inserted}$, which is simply because using ORNL data gives a higher β_{lost} than using JEF data, as seen in chapter 5.

4.3 Benchmark 3: Fuel-pump coast-down transient

4.3.1 Explanation of the benchmark

In this zero-power transient initial conditions are the steady state solution for the case the fuel is being pumped around at nominal flow speed and the core is critical (at t = 0, $g(0) = g_{nom} = 80.247 * 10^3\ cm^3/s$). When the fuel pump is now turned off at t = 0 the fuel-salt flow-rate starts to drop and becomes zero after approximately 15 seconds. During this time precursors stop leaving the core, causing the reactivity in the core to rise. Reactivity has to be withdrawn from the core by inserting a control rod to keep the reactor core critical (and at constant power). In this benchmark the reactivity that needs to be withdrawn as a function of time to keep the core critical is calculated and compared to the measurements done in the MSRE, and calculations done by the EDF computer code in the MOST study.

The steady state solution found in the calculation of β_{lost} due to fuel flow for nominal flow speed (section 4.1) was used as the initial condition for the values of N and $C_{i,j}$.

The fuel-salt flow-rate $g(t)$ during the fuel-pump coast-down transient was again evaluated from a graph [3, figure 2.11], in which the coolant-salt flow-rate and pump-speed where plotted as well as the fuel-salt pump-speed during the pump coast-down transient. This time a number of points were chosen on the graph of the coolant-salt flow-rate, and these points were adjusted for the faster fuel-pump coast-down speed, after which linear interpolation was used to evaluate the fuel-salt flow-rate at all times. The fuel-salt flow-rate $g(t)$ during fuel-pump coast-down is plotted in figure 4.4 (for details see appendix 7.3).

The reactivity inserted, $\rho_{inserted}$, to keep the reactor core critical is initially at the value of β_{lost}, and during the transient is again calculated with equation (4.2.1), with $\rho_{rod}^{n+1} = \rho_{inserted}$ at time $t = \Delta t(n+1)$.

The benchmark was run for U-235 fuel, using both ORNL (fig 4.4) and JEF (fig 4.5) precursor decay data.

4.3.2 Results and discussion

The benchmark was run with time step Δt = 0.01 s and for 70 s. The speed of the withdrawal of reactivity from the core did not have to be restricted since it never exceeded the maximum of 29.41 pcm/s.

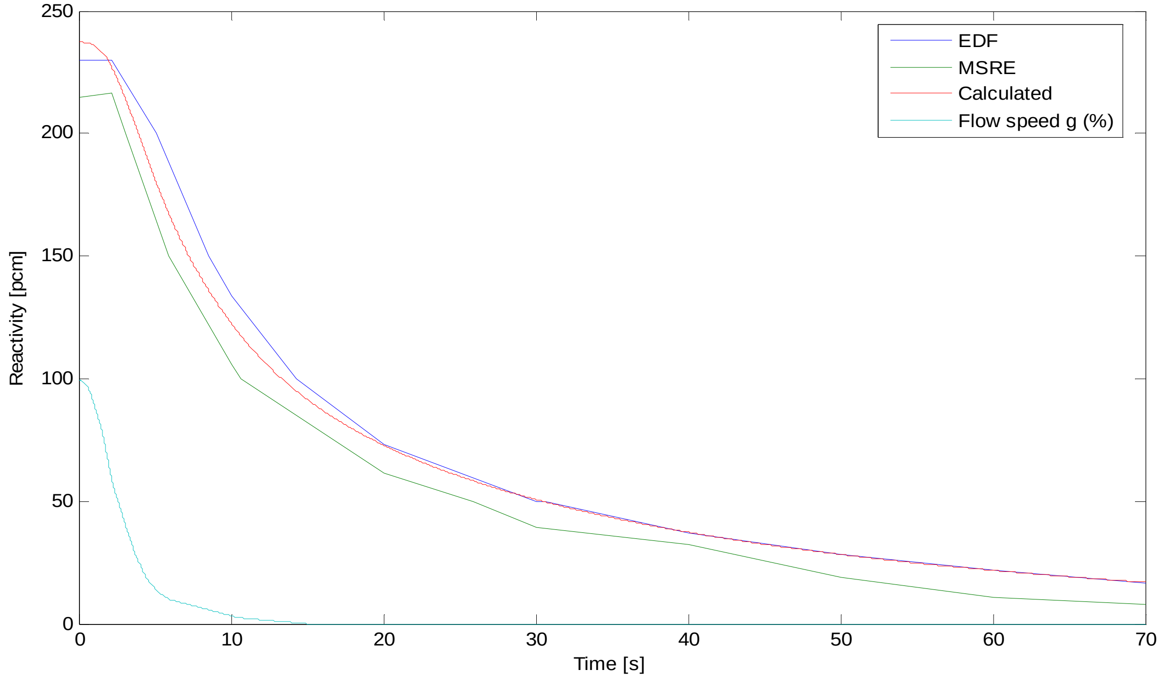

Figure 4.4: *Reactivity inserted during fuel-pump coast-down transient using ORNL precursor decay data. As calculated by our code, calculated by the EDF code in the MOST study [4] and measured in the MSRE. Also plotted is the flow-rate of the fuel-salt in percentage of nominal flow-rate.*

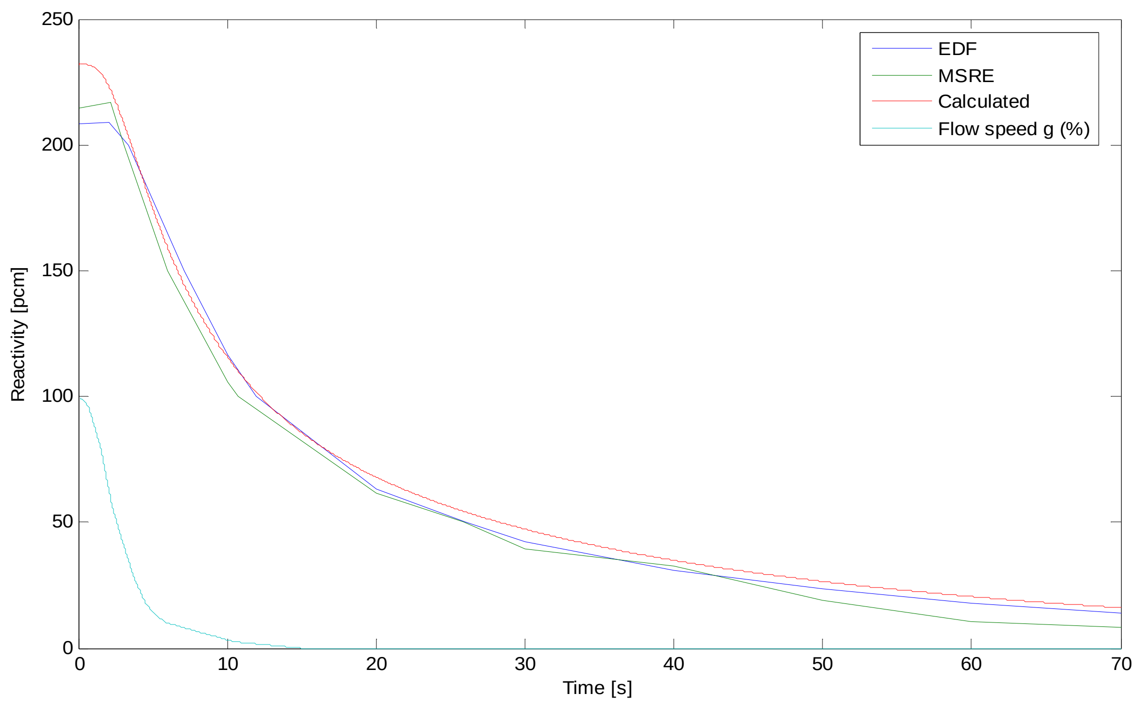

Figure 4.5: *Reactivity inserted during fuel-pump coast-down transient using JEF precursor decay data. As calculated by our code, calculated by the EDF code in the MOST study [4] and measured in the MSRE. Also plotted is the flow-rate of the fuel-salt in percentage of nominal flow-rate.*

4.3.3 B: Fuel-pump coast-down transient

As can be seen in figures 4.4 and 4.5, the calculated transient of the reactivity lost during fuel-pump coast-down followed that measured in the MSRE and calculated by the EDF code nicely. Since the fuel-salt flow-rate is (almost) zero during most of this transient, the simplifications in the fuel-salt flow model have only a small effect on the largest part of the transient. It is interesting though to note that the calculated transients follow the measured values in the MSRE even for the first 5 to 10 seconds of the transient, where the flow-rate rapidly changes. It seems that as opposed to transients involving an increase in the fuel-salt flow-rate, which causes strong oscillations in the reactivity not observed in the measurements in the MSRE, the calculation tool has no problem with transients involving a decreasing the flow-rate. The reactivity inserted at the start of the transient was of course the same as found in the calculation of β_{lost}, which is a bit higher then the value found in the MSRE. $\rho_{inserted}$ stayed slightly larger than that found in the MSRE, but was almost the same as the value calculated by the EDF model.

4.4 Benchmark 3: Natural convection transient

4.4.1 Explanation of the benchmark

Data of only one transient with thermal feedback was available, a natural convection transient using U-233 fuel. This transient will be used to evaluate the ability of the calculation tool to retrace transients in the power range where reactivity feedbacks from changing fuel and graphite temperatures in the core play a role.

During the natural convection transient at the MSRE the fuel pump was turned off and the only source of the fuel-salt flow-rate was natural convection due to the temperature difference between the core inlet and outlet temperatures. Initially the power generated by fission inside the core was only 4 kW, the fuel-salt flow-rate was almost zero and everything was at steady state. The transient was driven by increasing the heat-removal rate from the fuel-salt in the heat exchanger in steps, with the reactor critical, waiting for the system to approach equilibrium before the next change in the heat-removal rate was made. This increase in the heat-removal rate caused a lowering of the fuel temperature at the core inlet. This had several effects. Lowering the core inlet temperature caused the average temperature in the core to drop, and since the temperature feedback of the fuel and graphite on the reactivity is negative, this increased the reactivity, which in turn cause an increase in the power generated inside the core. This increase in power caused the fuel temperature at the core outlet to rise. Both the lowering of the fuel temperature at the core inlet and its rise at the core outlet raised the temperature difference between the core inlet and outlet temperatures, resulting in a higher fuel-salt flow-rate due to natural convection, since the convective flow was driven by the temperature difference over the reactor core.

During the transient, the fuel temperatures at the core inlet $T_{in}(t)$ and outlet $T_{out}(t)$ were measured as well as the reactor power $P(t)$. From these values and the specific heat c_p and density ρ of the fuel-salt, the fuel-salt flow-rate $g(t)$ was calculated with $g(t) = P(t)/\rho c_p(T_{out}-T_{in})$.

In the steady state situation the total reactivity change as compared to the starting condition, which was also a steady state, must be zero. The total reactivity change is given by

$$\Delta\rho = \Delta\rho_{flow} + \Delta\rho_{fuel} + \Delta\rho_{graphite} \tag{4.3.1}$$

with $\Delta\rho_{flow}$ the reactivity change due to fuel flow, $\Delta\rho_{fuel}$ the reactivity change due to temperature feedback from the fuel-salt, and $\Delta\rho_{graphite}$ the reactivity change due to temperature feedback from the graphite. From the plant data it was observed that the average fuel temperature inside the core decreases as the transient progresses in time. This implies a positive $\Delta\rho_{fuel}$ since the fuel temperature reactivity feedback coefficient is negative. $\Delta\rho_{flow}$ is negative because of the increase of the fuel flow from $0.06 \cdot 10^3$ cm^3/s to $1.70 \cdot 10^3$ cm^3/s. Finally, $\Delta\rho_{graphite}$ is also negative as a result of the rise of the graphite temperature. This is due to the fact that, as the power inside the core rises, more fission heat is deposited inside the graphite, which raises the graphite temperature. (Remember that the graphite is cooled by the fuel-salt, and thus has a higher temperature than the fuel).

In the original experiment during the MSRE the core inlet temperature was lowered by increasing heat-removal rate in the heat exchanger. Since detailed data on the heat exchanger used in the MSRE was not available, and for simplicity, a heat exchanger model was not used in the calculation of this transient. The fuel temperature at the core inlet $T_{in}(t)$ was used as the forcing function of the transient and $T_{in}(t)$ was given as a known input function for the computer model. This meant that in the computer model in the calculation of the fuel-salt temperature $T(z,t)$, the temperature of the volume element right before the core inlet was set to $T_{in}(t)$ at every time step. Another simplification was used for the fuel-salt flow-rate $g(t)$ resulting from natural convection. This can be calculated from the temperature difference over the core, but this is no trivial matter. So for simplicity $g(t)$ was also modeled as an input function. $T_{in}(t)$ and $g(t)$ were evaluated by linear interpolation of the data gained from the measurements in the MSRE [3, table 2.3].

Two different models of the core geometries were used in this benchmark: Initially calculations were performed with a purely homogeneous core model as given in figure 2.4. Afterwards, a geometric model was used which was closer to the actual reactor core geometry of the MSRE and to the model used in the MOST project [4], to see how this would affect the results. In this secondary model the graphite matrix was located in the central part of the core and the upper and lower 'plenum' contained only fuel salt and no graphite (figure 4.6).

As noted before in our computational model the fuel and graphite temperatures are not calculated separately, but assumed equal. In the homogeneous core model the total reactivity feedback of the fuel and graphite combined was calculated using (3.5.1) and one reactivity feedback coefficient, $\alpha = \alpha_{fuel} + \alpha_{graphite}$. For the non-homogeneous core model this gives a problem since α is no longer uniform throughout the whole core. This meant that the reactivity feedback from the graphite and the fuel salt had to be calculated separately with

$$\rho_{graphite}^{n+1} = \alpha_{graphite}\left(\sum_{j}^{\substack{\text{elements}\\ \text{containing}\\ \text{graphite}}} \left(f_j T_j^{n*}\right) - T_0\right) \tag{4.3.2}$$

$$\rho_{fuel}^{n+1} = \alpha_{fuel}\left(\sum_{j}^{core}\left(f_j T_j^{n*}\right) - T_0\right) \tag{4.3.3}$$

here the temperature reactivity feedback from the graphite is $\rho_{graphite}^{n+1}$ and the average weighted graphite temperature is calculated by summing over only those volume elements containing graphite. ρ_{fuel}^{n+1} is the temperature reactivity feedback from the fuel-salt. The total reactivity feedback due to temperature change ρ^{n+1} is simply $\rho_{graphite}^{n+1} + \rho_{fuel}^{n+1}$.

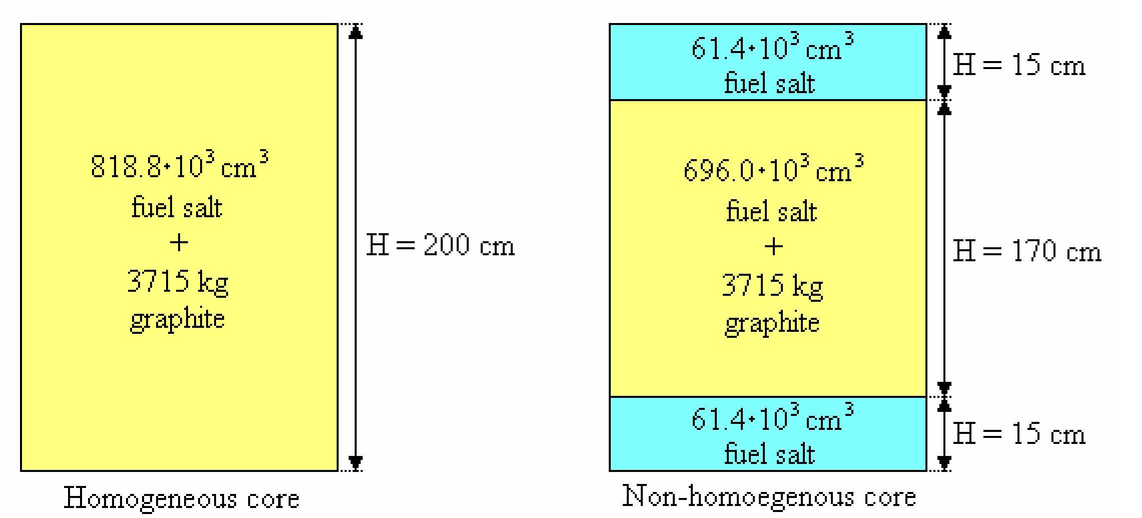

Figure 4.6: Geometrical model of the two different core-layouts used in the calculations of the natural convection transient. The area through which the fuel salt flowed, perpendicular to the flow direction, was the same everywhere: A = 4094 cm^2.

The reactivity feedback due to fuel flow, $\Delta\rho_{flow}$, for the different flow-rates during the transient was also calculated in this benchmark (see figure 4.7). The same method was used as in the calculation of the reactivity lost due to the fuel flow as a function of the fuel flow (section 4.1). The calculated results were compared with those given in the MOST project [4]. How $\Delta\rho_{flow}$ was obtained in the MOST study is unknown. It was certainly not data from measurements in the MSRE.

4.4.2 Results and discussion

4.4.2.1 Reactivity lost due to fuel flow for small flow rates

The reactivity lost due to fuel flow, $-\Delta\rho_{flow}$, as a function of the fuel flow for the flow regime in the natural convection transient was calculated for U-233 fuel using both JEF and ORNL precursor decay data. The results are plotted in figure 4.7 together with reactivity lost given in the MOST report. (For exact numbers, see table 7.4)

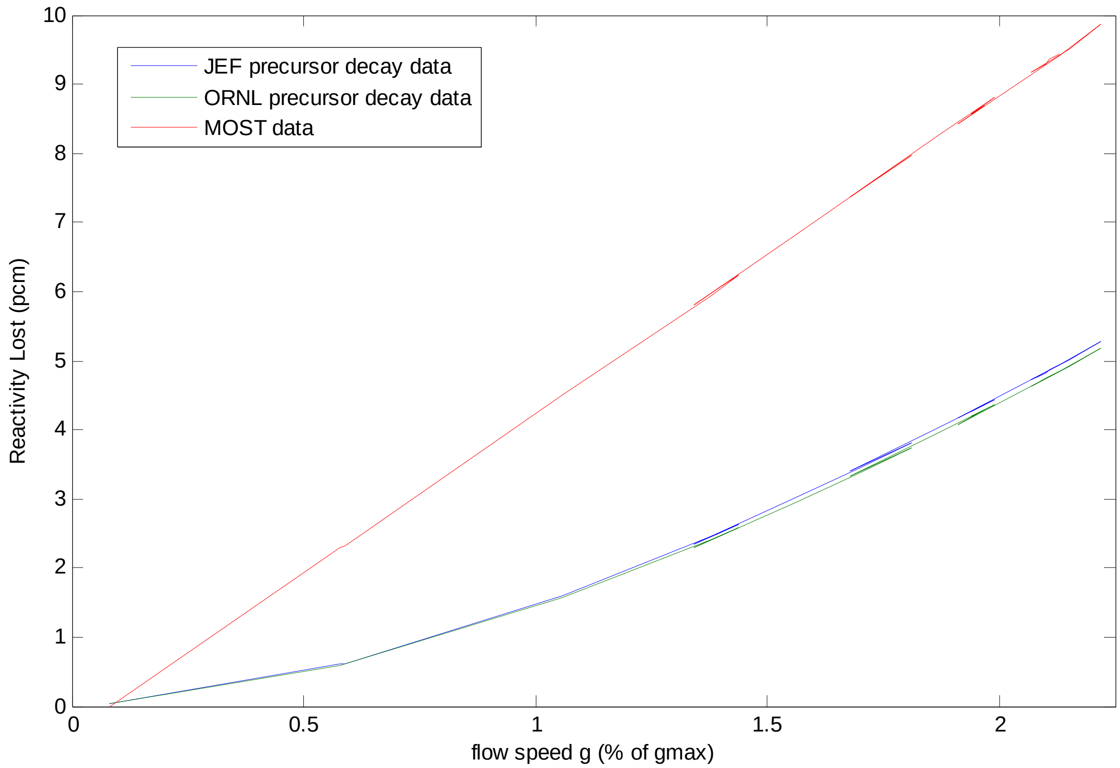

Figure 4.7: Reactivity lost due to fuel motion for the flow speeds during the natural convection transient as calculated by the computational model for U-233 fuel using JEF and ORNL precursor decay data, and data taken from [4].

There is a huge difference between the calculated reactivity lost due to fuel motion at the fuel-salt flow-rates during the natural convection transient. The reactivity values given in [4] are over twice as high as those calculated in the present work! Also the shape of the MOST values is linear, while the calculated reactivity loss rises exponentially with increasing fuel-salt flow-rate. The values given in MOST are not measured in the MSRE, but somehow derived by the writers of the MOST study. Unfortunately without an explanation how this was done. We will focus on trying to explain the shape of the calculated $-\Delta\rho_{flow}$.

All fuel flow-rates in this calculation were so small that there was no recirculation of precursors. The time that passed before the fuel reentered the core at the fastest flow-rate in the calculation (1781 cm^3/s) was 675 s. The longest living precursor group had a λ_i of 0.0126 s^{-1}. So by the time the fuel-salt reentered the core, only 0.02% of the precursors leaving the core were left, and of the other precursor groups an even smaller fraction. So all precursors swept out of the core had decayed by the time the fuel-salt reentered the core.

The following arguments support the shape of the exponential rise of $-\Delta\rho_{flow}$ at increasing fuel-salt flow-rates. Given that the fission power shape is sine shaped, the distribution of the precursors will also be sine shaped over the core. If the fuel-salt flow-rate has a certain speed, the precursors closest to the core outlet will be swept out of the core. Now if the flow-rate is twice as fast, precursors from twice as far from the core exit will be swept out of the core. Since the precursor distribution is sine shaped over the core, the further you get from the edge of the core, the higher the precursor concentration will be. This means that when the flow-rate doubles, the amount of precursors that get swept out of the core more then doubles. Thus the reactivity lost also more then doubles for a doubling of the flow-rate. At least until your flow-rate gets so high that precursors from the lower half of the core get swept out of the core and as long as there is no recirculation. But with the very low flow-rates in the natural convection transient, this is not the case.

Given that there is no explanation as to the origin of the values of $-\Delta\rho_{flow}$ given in [4], and in the light of the arguments given above, we have more confidence in the calculated values for $-\Delta\rho_{flow}$ due to fuel motion for low fuel-salt flow-rates then in those from the MOST study. The fact that the code performed well in the calculations of the reactivity lost due to fuel motion in the first benchmark, and actually gave values that were too high, also supports this conclusion. Finally, the linear shape of the data from MOST seems to indicate a simplification and the fact that the graph doest go through zero at zero flow-rate isn't physically sound either.

4.4.2.2 Natural convection transient

The reactivity feedback equilibrium temperature T_0 for the fuel and graphite was given [4 table 2.3] as T_0 = 1169.7 ^{o}F, or 632.06 ^{o}C. The reactor power during the natural convection transient was calculated for U-233 fuel, using both ORNL and JEF precursor decay data, for both a homogeneous and non-homogeneous core model.

As initial conditions the steady state solution was calculated, with the inflow temperature T_{in} set at the inflow temperature at $t = 0$ ($T_{in}(0)$ = 625.22 ^{o}C) and the flow speed g also set at its initial value $g(0)$ = 64 cm^3/s. Because of the very small flow rate, the simulation had to run a very long time, 500.000 s with Δt = 1 s, before the steady state solution was reached. See table 4.3 for the results.

The natural convection transient was calculated with time step Δt = 0.1 s. Tests (figure 10.2) showed that a smaller time step (0.02 s) gave the same results, so the time step was sufficiently small.

Table 4.3: Initial power P, core outlet temperature T_{out}, and reactivity lost due to fuel flow $\Delta\rho_{flow}$, as calculated with the computational model in the four different situations and as measured in the MSRE.

	$P(0)$ [kW]	$T_{out}(0)$ [°C]	$\Delta\rho_{flow}(0)$ [pcm]
MSRE data	4.1	638.89	0.00
JEF non-homogeneous core	3.82	638.48	-0.0414
JEF, homogeneous core	3.82	638.49	-0.0414
ORNL, non-homogeneous core	3.82	638.48	-0.0412
ORNL, homogeneous core	3.82	638.49	-0.0412

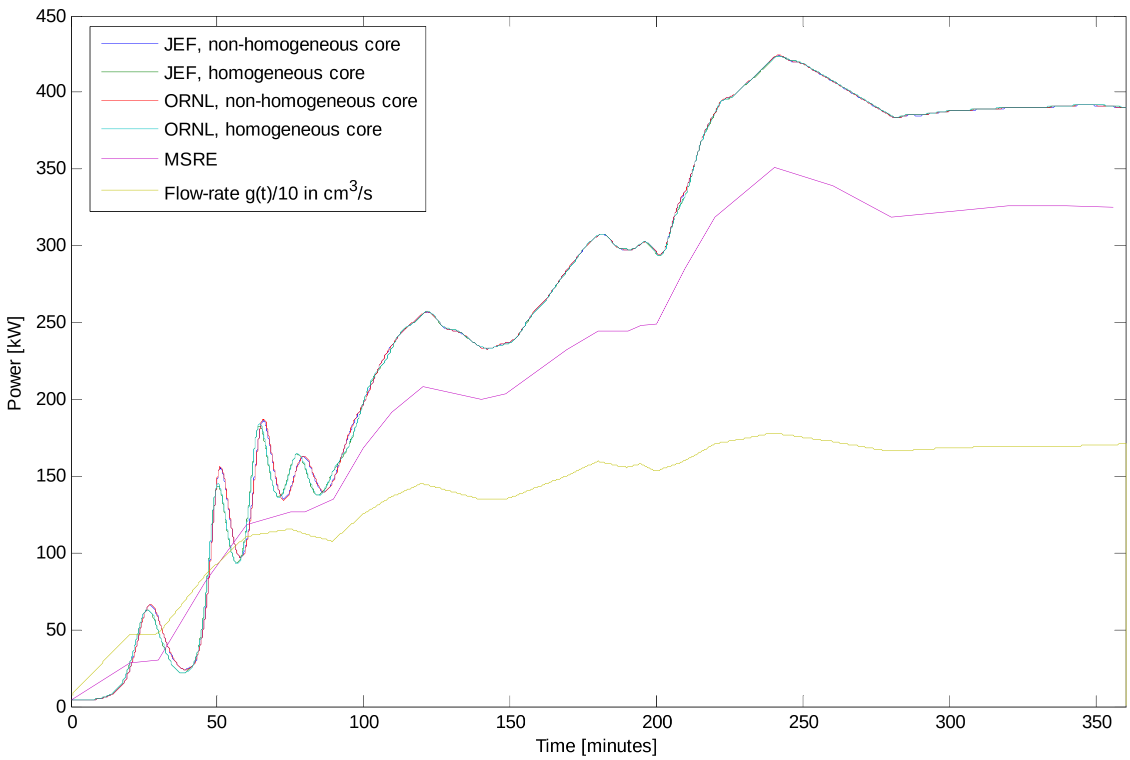

Figure 4.8: Natural convection transient reactor power P in time. The four results generated by the model for the different input values (homogeneous core and non-homogeneous core, with ORNL or JEF precursor decay data) and the experimental result from the MSRE. Also included is the fuel-salt flow-rate g(t) in cm^3/s, divided by 10.

If we look at the plot of the reactor power versus time (figure 4.8) and compare it with the results from the MSRE a couple of things can be noted. First, the shape of the power curve is the same as that of the power in the natural convection experiment in the MSRE. The second thing is that although the shape is almost identical, the power level is approximately 20% too high at all times. Furthermore, in the first part of the transient the calculated power oscillates strongly, as opposed to the measured power in the MSRE. Also, the results for the JEF precursor data and the ORNL precursor data are identical. The difference in the calculated reactor powers for the homogeneous core and the non-homogeneous core geometry model is only evident in the first part of the transient, where the power and reactivity are fluctuating wildly and the situation is far from steady state.

Even here the difference is small After 100 minutes have passed all four calculations give the same reactor power.

From the calculation of $\Delta\rho_{flow}$ versus the fuel speed for the ORNL and JEF precursor data (figure 4.7) one can conclude that the difference in $\Delta\rho_{flow}$ between the two data sets is less than two percent in this regime, or only 0.1 pcm. To compensate, at steady state reactivity feedback from the fuel and graphite temperatures ($\Delta\rho_{fuel} + \Delta\rho_{graphite}$) will also differ only 0.1 pcm maximal, which means a change of the average core temperature of $0.1/\alpha_{total}$ = 0.007 °C (with α_{total} = 15.3 pcm/°C). Given these facts, it is no surprise that there is no visible difference in the fission power in time between these two data sets.

There is a slight but noticeable difference in the power calculated for the two different core geometries. This difference disappears when the calculated power stops oscillating after about 100 minutes. The different geometries have two effects: First the reactivity feedback coefficient for the non-homogeneous core in the upper and lower part is different from that of the homogeneous. And second, in the non-homogeneous core geometry the total heat capacity in the volume elements in the plenums is lower and in the central part of the core is higher than in the homogeneous situation. The difference in the reactor power of the two different core geometries is only evident in the part where the system is fluctuating wildly, and is thus far from steady state. At later times the two situations have again identical solutions. This can be explained as followed. First, the reactivity feedback coefficient α for the central part of the core does not change. Only at the boundaries is this changed between the 2 geometries. Since the fission shape is sine shaped, the areas near the boundaries contribute very little to the fission process, and the effect on the power of a change in reactivity here (from a different feedback coefficient) will be very small. Secondly, the total heat capacity of the volume elements only affects the system when it is not in steady state. It determines how fast the temperature in the given volume cell will change. The heat capacity has no influence on the steady state solution itself, where the temperature is constant. So after the first 100 minutes of the transient have passed, and the system is almost always very near to or in steady state and there are no abrupt temperature changes in time, the effect of the different heat capacities is negligible.

Oscillations in the power could be expected. As the fuel inlet temperature is lowered, positive reactivity is inserted in the reactor core. Because of this the reactor power will rise and the fuel temperature will rise. Until the temperature rise causes enough negative reactivity feedback to compensate, and the reactivity is zero again. At this point however, the temperature will still be rising because of a high power (higher then in the steady state situation). Now the temperature will keep rising, and the reactivity dropping, causing in turn the power to drop. This in turn will cause the temperature to stop rising and then dropping, until reactivity is zero again. But now the power will be to low to sustain the current temperature with the given fuel flow! And the cycle starts again. This will cause oscillations in the power around its steady state value. In time the oscillations in the power will dampen out to the steady state situation. In figure 4.8, fluctuations of the reactor power at every major rise in the power can be observed, but they are far more pronounced in the beginning of the transient. Because of very slow fuel flow here, it takes more time to adjust to the new situation. Also, the functions driving the transient (inflow temperature and fuel-salt flow-rate) change more rapidly in the first part of the transient, causing more abrupt changes in the reactor core. In the MSRE mixing of the fuel-salt due to local differences in the flow-rate dampens out the oscillations. Not only because it distributes the precursors more evenly, as discussed in the benchmark concerning fuel-pump start-up transient, but also because it distributes the heat more evenly throughout the reactor core and will speed up the transport of heat throughout the reactor, thus letting the temperature rise more evenly throughout the reactor core than it does in the calculated case.

Finally, why is the calculated fisson power too high? The transient can be evaluated in reactivity's. There is a negative reactivity insertion by the fuel flow, $\Delta\rho_{flow}$, which has to be compensated by a temperature feedback on the reactivity from the fuel and graphite temperatures ($\Delta\rho_{fuel}$ and $\Delta\rho_{graphite}$), resulting, for steady state, in a total reactivity change of zero:

$$\Delta\rho = \Delta\rho_{flow} + \Delta\rho_{graphite} + \Delta\rho_{fuel} = 0 \tag{4.3.4}$$

$\Delta\rho_{fuel}$ and $\Delta\rho_{graphite}$ can be expressed as:

$$\Delta\rho_{fuel} + \Delta\rho_{graphite} = \alpha_{fuel}\left\langle \Delta T_{fuel} \right\rangle + \alpha_{graphite}\left\langle \Delta T_{graphite} \right\rangle \tag{4.3.5}$$

where the ΔT's represent a temperature difference from T_0. In the calculated case, the fuel and graphite temperatures are the same, but in the MSRE, they were not. $T_{graphite}$ was higher than T_{fuel}, since the fuel-salt is also the coolant and has to cool the graphite. This means $\Delta\rho_{graphite}$, was lower in the MSRE then in the calculated case (since $\alpha_{graphite}$ is negative). This means $\Delta\rho_{fuel}$ was higher than calculated in the steady state situation in the MSRE, and for this to happen T_{fuel} must have been lower. With a fixed inflow temperature, a lower fuel average temperature means a lower fuel outflow temperature. With a fixed flow speed this in turn means less power is generated inside the reactor, since the total power generated is equal to $g\rho c_p(T_{out} - T_{in})$.

5 Conclusion and recommendations

In the present study the development of a computational model of a molten salt reactor is described. This model was then tested by simulating various experiments performed during the Molten Salt Reactor Experiment. In these benchmarks the results of the developed computational model were compared with the experimental results from the MSRE. Also a comparison was made with the results of a similar computational model, the EDF model, detailed in the MOST report [4]. These comparisons allowed for a thorough testing of the computational model.

From the first benchmark, the evaluation of reactivity lost due to fuel motion, it can be concluded the developed code can reasonably well calculate steady state values in the zero-power regime. The calculated values are 10% to 20% too high, but in light of the simplifications used in the modeling, were acceptable. Also, the calculated reactivity lost due to fuel motion as a function of fuel flow-rate shows the expected behavior. It was noted that taking different fission and adjoint flux shapes has a strong impact on the numerical value of the reactivity lost due to fuel motion. In the developed model, these shapes are very simple, only a flat or a sine shape is considered. A flat adjoint flux shape and a sine shaped fission shape were found to give results best in agreement with the measurements done during the MSRE. Calculating the adjoint flux and fission shapes in detail could probably improve the value of the calculated reactivity lost due to fuel motion. Another factor which probably influenced the calculated reactivity lost due to fuel motion was the fact that in the model only variations in the z (flow) direction were taken in consideration.

The fuel-pump start-up benchmark (section 4.2) shows that when the fuel-salt flow-rate rises, the computational model has some small problems in calculating the transient. The general behavior of the fuel-pump start-up transient was followed, but the calculated reactivity fluctuated strongly around its equilibrium value and took a relatively long time to stabilize, where in the measured transient at the MSRE the reactivity due to fuel motion quickly stabilized at its steady state value. Also, the observed overshoot in the reactivity in the MSRE was a lot bigger in the calculated results. These fluctuations and larger overshoot were expected though with the used physical model. A simplified flow model, with a plug flow (uniform flow speed everywhere) in the whole reactor was used. In the real situation there must have been at least some differences in flow speeds and some mixing of the fuel-salt in the fuel-pump and upper and lower plenums. This would cause the precursor concentrations to be distributed more evenly during the transient and dampen fluctuations.

The third benchmark, the fuel-pump coast-down transient, showed that the computational model has no problem in calculating transients in which the fuel-salt flow-rate is lowered.

The last benchmark, the natural convection transient, shows that the code performs quite well in the power regime, with temperature feedback on the reactivity and thermal-hydraulic calculations included in the code. The shape of the transient is followed nicely, with two major deviations. There were strong fluctuations in the calculated power, from fluctuations in the reactivity, in the first part of the transient, but the trend still followed the transient. In this part, the fuel-salt flow-speed increased relatively fast. As was seen in the fuel-pump start-up transient (section 4.2), this resulted in strong fluctuations in the reactivity. The calculated power was roughly 20% too high at almost all times. This is probably due to the fact that the computational model does not calculate the graphite and fuel temperatures separately, but uses the same temperature for both. In reality, the fuel temperature will be lower than the graphite temperature, so the calculated fuel temperature will be too high. In the case of the natural convection transient, since the inflow temperature is fixed, this leads to a higher calculated power than in the MSRE.

It can be concluded that the present calculation tool performs well for the calculation of steady states, both in the zero power regime as with temperature feedback. The calculated reactivity lost due to fuel motion was 15% (U-235) to 20% (U-233) too high and in the power regime the fuel temperature will always be calculated too high, 20% in the case of the natural convection transient. Considering the simplifications made in implementing this code, these errors are acceptable. For the calculations of transients the tool has problems when the fuel-salt flow-rate rises rapidly, as compared to the actual flow-rate. This will cause the calculated reactivity in the transient to fluctuate strongly around the equilibrium value, while these fluctuations were not observed or a lot smaller in the experimental case. Lowering of the flow-rate does not cause any problems. Apart from these fluctuations, the code can calculate transients in both the zero-power as well as in the power regime quite correctly, retracing the shape of the transients of the experimental date without problems, although the actual numerical results will have the same errors as in the steady state calculations.

The computational model is well suited to calculate both transients and steady state solutions for a molten salt reactor, especially when the weak points mentioned above are taken in consideration. However, if precise numerical values are needed or detailed (peek) values for transients, a more detailed model is required.

Recommendations for further improvements

First the shape of the adjoint flux and fission shape should be calculated more precisely, maybe by a different computational tool, to improve the calculated reactivity lost due to fuel motion. Ideally this should be done in 3D, since in the current model it was assumed the radial shape of the adjoint flux and fission shape did not change with the z location. The error made by this assumption is unknown though and requires study.

Also the graphite and fuel-salt temperatures should be calculated separately, which also means calculations for the transfer of heat between the graphite and fuel-salt have to be included in the code. This will strongly improve the numerical results on the calculation of the fuel-salt temperature in the power regime. Since the heat transfer between the graphite and the fuel-salt depends on the fuel-salt flow this is no trivial job, and also leads to the next recommendation.

To allow for detailed heat transfer calculations between the graphite and the fuel salt, and to remove the strong fluctuations in the calculated reactivity in transient calculations when the fuel-salt flow-rate rises rapidly, a more detailed implementation of the fuel-flow is needed. Including a diffusion term in the flow model to accommodate for non-uniform flow-rates might already help, but the implementation of a detailed flow model, including radial variations, is recommended. Especially in the reactor core variations in the flow-speed at the different radial positions are expected and could have an important effect on calculated results. Also a detailed model of the mixing of the fuel-salt in the pump and plenums is advised.

Finally, as can be seen from the previous recommendations, ideally a computational model including both axial as well as radial variations of all variables of interest should be made of the MSR. This code should include detailed calculations of the fission and adjoint flux shapes, separate calculation of the fuel-salt and graphite temperatures and a model of the mixing of the fuel-salt in the pump and plenums.

6 References

[1] Wikipedia, http://en.wikipedia.org/wiki/Generation_IV_reactor, Generation IV reactor, February 2007.

[2] D. Lathouwers & others, lecture notes nuclear reactor physics, 2nd half 2006.

[3] P.N. Haubenreich and J.R. Engel, Experience with the Molten-Salt Reactor Experiment, *Nuclear Applications and Technology* 8: 118–136, 1970.

[4] MOST: Review of Molten Salt Reactor Technology, *European Commission, 5th euratom framework programme 1998-2002*, July 2003.

[5] Weston M. Stacey, Nuclear Reactor Physics, Wiley-VCH, Weinheim, 2004.

[6] E. Anderson et al., LAPACK Users' Guide third edition, *Society for Industrial and Applied Mathematics*, Philadelphia, PA, 1999.

[7] J. Kophazi, M. Szieberth, S. Feher, Gy. Csom, P.F.A. de Leege, MCNP based calculation of reactivity loss in circulating fuel reactors, *Nuclear Mathematical and Computational Sciences: A century in Review, A Century Anew*, Gatlinburg, Tennessee, April 2003.

[8] Jozsef Kophazi, Danny Lathouwers, Jan Leen Kloosterman, Sandor Feher, Three-dimensional space and time-dependent analysis of molten salt reactors, *PHYSOR-2006*, Vancouver, Canada, September 2006.

[9] Jiri Krepel, Ulrich Grundmann, Ulrich Rohde, Frank-Peter Wiess, DYN1D-MSR dynamics code for molten salt reactors, *Annals of Nuclear Energy* 32 (2005) 1799-1824.

7 Appendix A: Additional calculation results

7.1 Reactivity lost versus varying fuel flow-rate

For the β_{lost} evaluation versus pump speed g, with $g_{nom} = 80.247*10^3$ cm^3/s, the calculation was run with time step Δt = 1 s and for a maximum of 1500 s. This was sufficient time to attain steady state for all flow-rates.

Table 7.1: β_{lost} versus the fuel flow as a fraction of nominal flow for U-233 and U-235 fuel, using ORNL and JEF precursor decay data. The time step Δt = 1 s.

	β_{lost} [pcm], Δt = 1 s			
g/g_{nom}	U-235 ORNL	U-235 JEF	U-233 ORNL	U-233 JEF
0.1	56.5993	53.1035	34.2804	33.2730
0.2	99.9755	94.1105	57.5622	55.1113
0.4	151.406	144.388	82.0584	80.4508
0.6	187.291	180.703	97.7675	97.8199
0.8	215.084	209.503	109.377	111.036
1.0	237.297	232.911	118.278	121.453
1.25	259.246	256.384	126.768	131.640
1.5	276.326	274.909	133.194	139.501
2	300.601	301.716	142.071	150.555
3	328.252	333.382	151.699	162.888

For U-233 fuel using ORNL precursor decay data at $g = g_{nom}$ it was tested if the time step Δt had an influence on the calculated β_{lost}. Calculations with Δt = 1, 0.1 and 0.01 s all converged to 118.278 pcm.

7.2 Estimation of the fuel-salt flow-rate during pump start-up

In [4, figure 2.10] the fuel pump-speed and coolant pump-speed were given. From this it was noted they had the same shape, but the coolant pump reached 100% after 1.6 seconds and the fuel pump after 1 second. From this it was reasoned the fuel-salt flow-rate would also have the same shape as the coolant-salt flow-rate [4, figure 2.11], but with a time-scale compressed by this same factor. The shape of the fuel-salt flow-rate was modeled to be of the form

$$g(t) = g_{nom} \cdot (e^{t \cdot \tau} - 1) \qquad (7.2.1)$$

for flow-rates up to 40%, and of the form

$$g(t) = g_{nom} \cdot (1 - e^{-(t - t0)/\tau 2}) \qquad (7.2.2)$$

for higher flow-rates.

A few points were taken from the coolant flow-rate, which were scaled for the faster fuel pump-speed with 1/1.6 (table 7.2) after which equations (7.2.1) and (7.2.2) were fitted on these data.

Table 7.2: Time versus flow-rate in % of nominal flow for the coolant-salt and the fuel-salt during pump start-up transient.

G [% of g_{nom}]	$t_{coolant}$ [s]	t_{fuel} [s]
80%	2.3	1.4375
60%	1.4	0.875
40%	0.9	0.5625

(7.2.2) was fitted on the data in table 10.1 which gave *τ2* = 0.793 and *t0* = 0.15625. By solving (7.2.1) = (7.2.2) at $t = 0.5625$, $\tau = 0.5993$ was found. The fuel flow-rate was taken 100% at $t > 10$ seconds. This all gave the following function for the fuel-salt flow-rate $g(t)$ during the fuel-pump start-up transient:

$$g(t) = \begin{cases} g_{nom} \cdot (e^{t \cdot 0.5993} - 1) & t < 0.5625 \\ g_{nom} \cdot (1 - e^{-(t-0.5625)/0.793}) & 0.5625 < t < 10 \\ g_{nom} & t > 10 \end{cases} \tag{7.2.3}$$

7.3 Estimation of the fuel-salt flow-rate during pump coast-down

In [4, figure 2.11] the fuel pump-speed and coolant pump-speed were given, as well as the coolant-salt flow-rate. To evaluate the fuel-salt flow-rate during fuel-pump coast-down from this figure, it was noted the fuel and coolant pump-speeds had the same shape, but the fuel pump-speed lowered faster in time. The coolant pump-speed took 16 second to reach zero and the fuel-pump speed 12 seconds.

Now several points were evaluated on the graph of the coolant flow-rate versus time. To get from these the times at which the fuel flow-rate had the same value, the time for each point was multiplied by 12/16 (see table 7.3). To get from these the fuel-salt flow-rate in time $g(t)$ during the fuel-pump coast-down transient, the values for the fuel-salt flow-rate from table 7.3 were linearly interpolated (see figure 7.1).

Table 7.3: Coolant flow-rate in % of nominal flow versus time from [3, figure 2.11] and fuel-salt flow-rate versus time as calculated from these values.

Coolant flow-rate [%]	Time [s]	Fuel flow-rate [%]	Time [s]
100	0.0	100	0.0
98	0.6	98	0.45
95	1.0	95	0.75
80	2.0	80	1.5
57	3.0	57	2.25
42	4.0	42	3.0
28	5.0	28	3.75
18	6.0	18	4.5
13	7.0	13	5.25
10	8.0	10	6.0
2.5	14.0	2.5	10.5
0	20.0	0	15.0

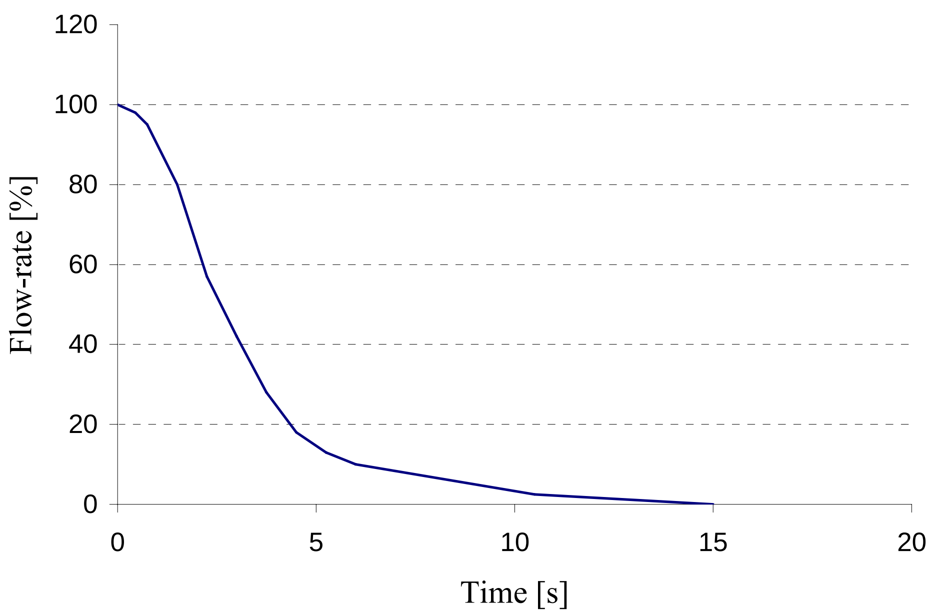

Figure 7.1: Fuel-salt flow-rate in percentage of nominal flow versus time during pump coast-down transient.

7.4 Natural convection transient

To test if the time step in the calculation of the natural convection transient (Δt = 0.1s) was chosen sufficiently small, the transient was also calculated with a smaller time step of Δt = 0.02 s. This was done for a non-homogeneous core model and both JEF and ORNL precursor decay data. The transient was only calculated for the first 80 minutes to safe time. (After 80 minutes the changes in power and temperature reactivity feedback were more gradually so the effect of a smaller time step was expected to be smaller).

Calculations for both time steps gave exactly the same results (figure 7.2), so a time step of 0.1 s was sufficiently small for our model.

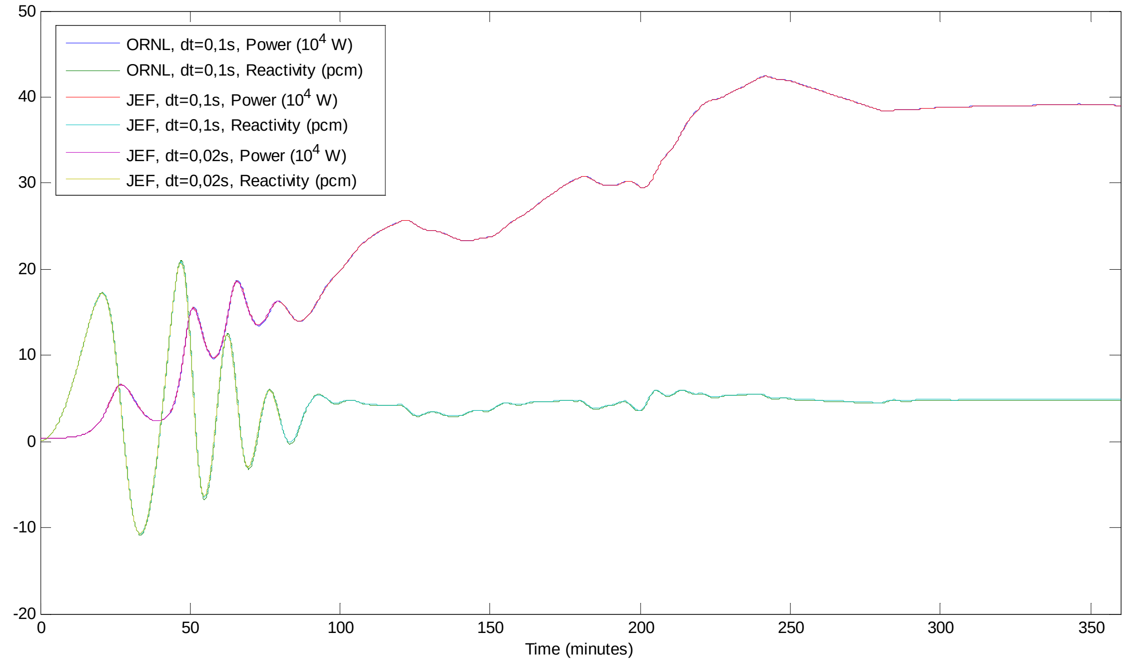

Figure 7.2: Power and reactivity feedback from fuel and graphite temperatures for the natural convection transient using the non-homogeneous core model, for both JEF and ORNL precursor data, calculated with a time step Δt = 0.1 s and a time step Δt = 0.01 (calculated only for t = 0 to 80 minutes).

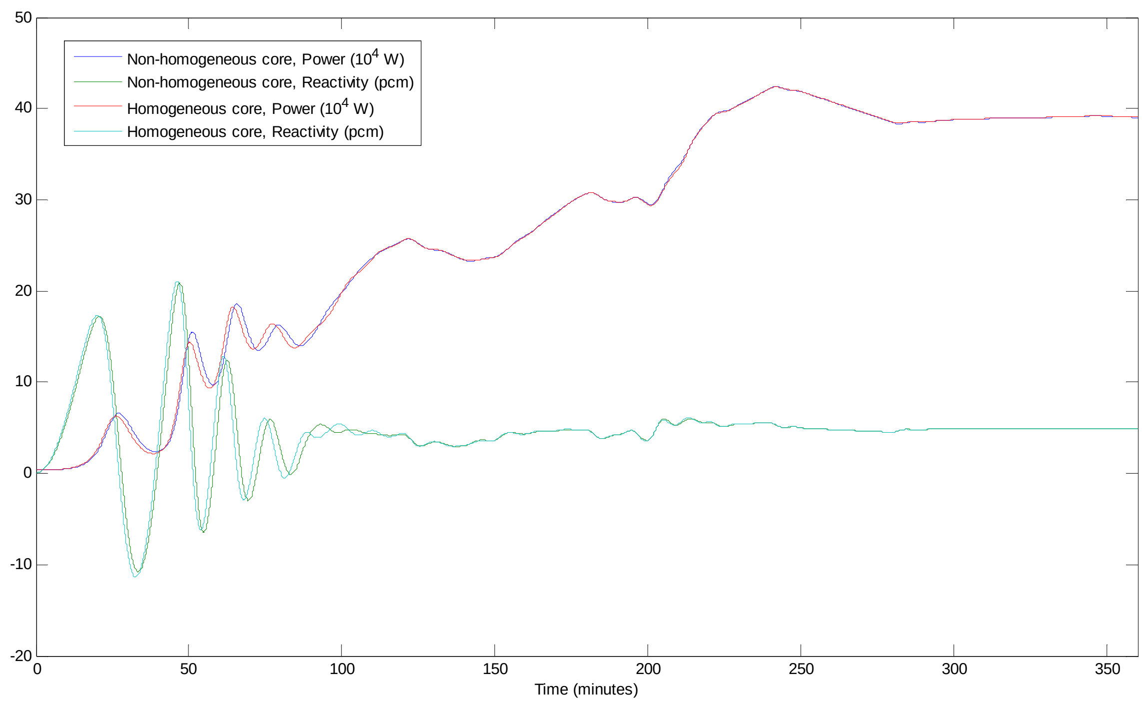

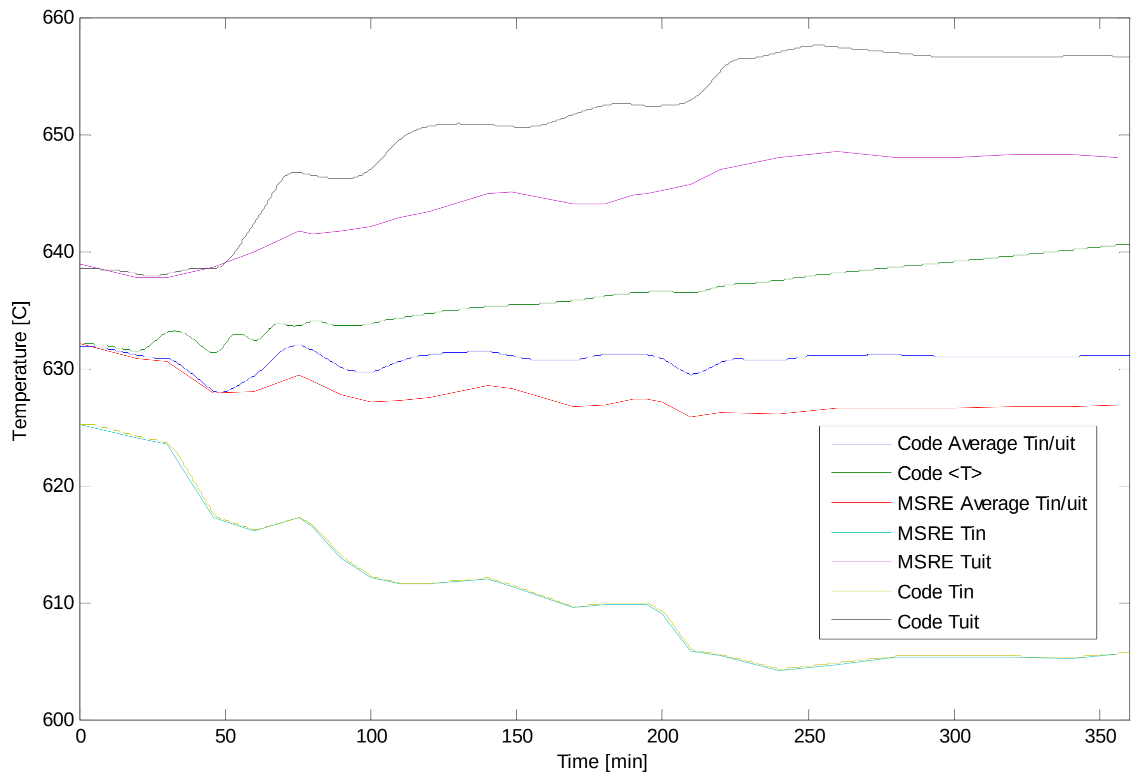
Temperature [C]
Time [min]
Code Average Tin/uit
Code <T>
MSRE Average Tin/uit
MSRE Tin
MSRE Tuit
Code Tin
Code Tuit

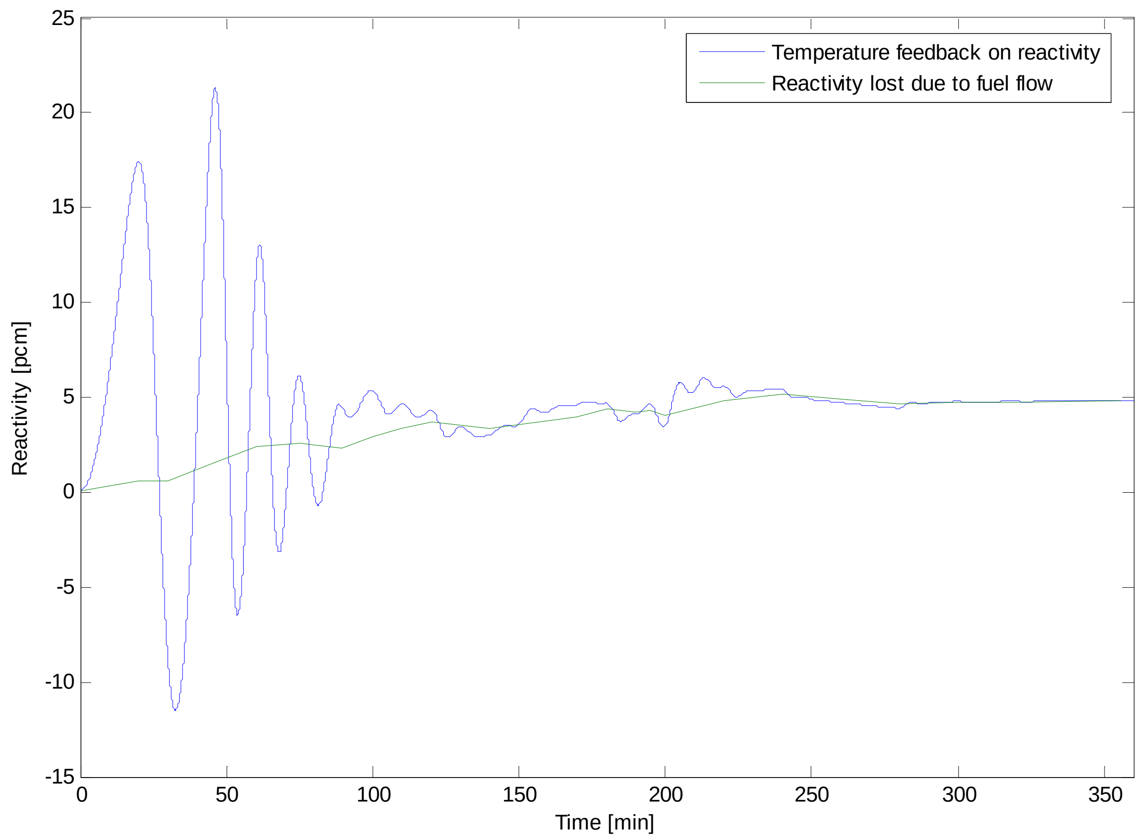
Reactivity [pcm]
Time [min]
Temperature feedback on reactivity
Reactivity lost due to fuel flow

Table 7.4: Reactivity lost due to fuel-salt flow-rate, for flow-rates in the natural convection transient. The reactivity lost was calculated for both JEF and ORNL precursor data, and the reactivity lost as given in [4] was also included.

Flow-rate [% g_{nom}]	Reactivity lost due to fuel flow [pcm]		
	JEF	ORNL	MOST [4]
0.08	0.0413831	0.0411754	0
0.58	0.607392	0.597048	2.29
0.59	0.623875	0.613187	2.33
1.06	1.60135	1.56986	4.50
1.38	2.46508	2.41605	5.95
1.44	2.64200	2.58956	6.23
1.40	2.52357	2.47340	6.08
1.34	2.34959	2.30282	5.80
1.56	3.00840	2.94915	6.81
1.70	3.45539	3.38831	7.46
1.81	3.81996	3.74689	7.98
1.68	3.39033	3.32435	7.37
1.87	4.02337	3.94712	8.25
1.99	4.43902	4.35669	8.80
1.94	4.26445	4.18461	8.57
1.97	4.36897	4.28762	8.68
1.91	4.16065	4.08233	8.42
2.13	4.93754	4.84860	9.42
2.22	5.26495	5.17210	9.87
2.15	5.00985	4.92002	9.51
2.07	4.72221	4.63602	9.16
2.10	4.82957	4.74199	9.29
2.11	4.86549	4.77745	9.36
2.13	4.93754	4.84860	9.44

8 Appendix B: MSR data

All the data for the molten salt reactor modeled in this study were taken from [4].

MSRE Fuel composition:
U^{235} salt composition (molar proportions): 65% LiF, 29.2% BeF_2, 5% ZrF_4, 0.8%UF_4
Uranium composition: 32% U^{235}, 68% U^{238}
All fission products and other heavy nuclei are neglected for the benchmark calculations

Table 8.1: U^{233} salt composition:

Isotope	Isotope proportion (normalized to 1)
F^{19}	5.961 E-01
Zr (natural)	2.033 E-02
Li^{17}	2.643 E-01
Be^{9}	1.187 E-01
U^{238}	1.859 E-05
U^{235}	9.274 E-06
Pu^{239}	8.894 E-06
U^{233}	4.437 E-04
U^{234}	4.370 E-05
Pu^{240}	4.132 E-07
Pu^{241}	3.220 E-08

Table 8.2: Neutronic data for U^{235} and U^{233} fuel.

Quantity	Dimension	U^{235}	U^{233}
α_{fuel}	Pcm/C	-8.46	-9.54
$\alpha_{graphite}$	Pcm/C	-4.68	-5.76
Neutron life-time l	S	0.000240	0.00040
β_{eff} (ORNL)	-	0.006661	0.002894
β_{lost}	Pcm	212	100.5 (±5%)
ρ_{fuel}	Kg/cm^3	$2263.0\cdot10^{-6}$	$2263.0\cdot10^{-6}$
C_{p_fuel}	J/kgK	1982.5	1982.5
$p_{/fiss}$	J / fission	$3.0864\cdot10^{-11}$	$3.046\cdot10^{-11}$
ν (Stacey p140)	# / fission	2.49	2.58

Table 8.3: ORNL precursor decay data.

	U^{235} fuel		U^{233} fuel	
Group	λ (s^{-1})	β_{eff} (10^{-5})	λ (s^{-1})	β_{eff} (10^{-5})
1	0.0124	22.3	0.0126	23.76
2	0.0305	145.7	0.0337	85.76
3	0.111	130.7	0.139	71.90
4	0.301	262.8	0.325	82.14
5	1.14	76.6	1.13	15.79
6	3.01	28	2.5	10.03
Total		666.1		289.38

Table 8.4: JEF precursor decay data.

	U^{235} fuel		U^{233} fuel	
Group	λ (s^{-1})	β_{eff} (10^{-5})	λ (s^{-1})	β_{eff} (10^{-5})
1	0.01272	25.93	0.01272	26.4
2	0.03174	133.35	0.03174	67.6
3	0.116	127.44	0.116	70.1
4	0.311	283.64	0.311	118.9
5	1.4	116.9	1.4	33.9
6	3.87	48.8	3.87	9.4
Total		736.06		326.3

Table 8.5: Graphite Data.

	Dimension	Value
$C_{p\ graphite}$ (at 1300 F)	J/kgK	1750.0
$\rho_{graphite}$ (at 1300 F)	kg/cm^3	$2180.0*10^{-6}$
Bulk Density	g/cm^3	1.82 – 1.87
Volume	cm^3	$1.954*10^6$
Total mass	kg	3715

Table 8.6: MSRE Plant geometry. Area is the area perpendicular to the flow direction through which fuel-salt flows.

	Height/Length (cm)	Fuel Volume (cm^3)	Area (V/H) (cm^2)
Core	65.5” = 166.37 cm	$0.6787\cdot10^6$	$4.080\cdot10^3$
Effective Core	79” = 200.66 cm	$0.8188\cdot10^6$	$4.080\cdot10^3$
Upper/Lower Plenum (part of core)	6.75” = 17.145 cm	$0.07005\cdot10^6$	$4.080\cdot10^3$
Outside core		$1.202\cdot10^6$	

Table 8.7: Modeled plant geometry (HE = heat exchanger).

	Height/Length (cm)	Fuel Volume (cm^3)	Area (cm^2)
Core	200	$0.8188\cdot10^6$	4094
Pipe Core-HE	400	$0.3005\cdot10^6$	751.25
HE	200	$0.6010\cdot10^6$	3005
Pipe HE-Core	400	$0.3005\cdot10^6$	751.25

For the calculation of the extrapolated height of the core, H_{ex}, the following equation is used:

$$H_{ex} = H + \lambda_{extrap} \tag{8.1.1}$$

where λ_{extrap} is the thermal extrapolation distance. In [5, p. 49] λ_{extrap} for C is given as λ_{extrap} = 1.95 cm, which results in H_{ex} = 201.95 cm.

Step size in the z-direction: $\Delta z = 5$ cm.
The fuel-salt flow-rate $w = 181.6$ kg/s or $g = 80.247*10^3$ cm^3/s.
Effective Fuel transit time in core = 10.28 s.
Effective Fuel transit time in external primary loop = 14.91 s.
Total primary circuit Transit Time = 25.19 s.

Heat exchanger data (for reactor at normal power):
Heat capacity = 0.4 MWs/F
Fuel-salt – heat exchanger heat transfer coefficient for the whole heat exchanger = 0.36 MW/F
Heat exchanger Outlet temperature = 1052 F = 566.7 ^{o}C
Heat exchanger Inlet temperature = 997 F = 536.1 ^{o}C
Length = 200 cm
Heat Transfer Area $OL = 25.937*10^4$ cm^2
Heat Transfer Coefficient $h = 0.3486$ W/cm^2K

9 Appendix C: Basic tests of the calculation tool

9.1 Check of $C_i(z)$ at steady state without fuel motion

For the evaluation of the reactivity lost due to fuel motion (section 4.1) the steady state situation with no fuel motion ($g = 0$) was calculated to use as initial conditions.
The calculated precursor concentrations inside the core can be compared with the theoretical solution. As mentioned in section 4.1, (4.1.1) gives the (discretized) analytical solution. By solving (2.3.6) we get $C_i(z)$ as a function of z (no fuel motion and steady state, so $g = 0$ and $\partial C/\partial t = 0$).

$$C_i(z) = \frac{\beta_{i,eff}}{\Lambda \lambda_i} \frac{f(z)N}{A(z)} \tag{9.1.1}$$

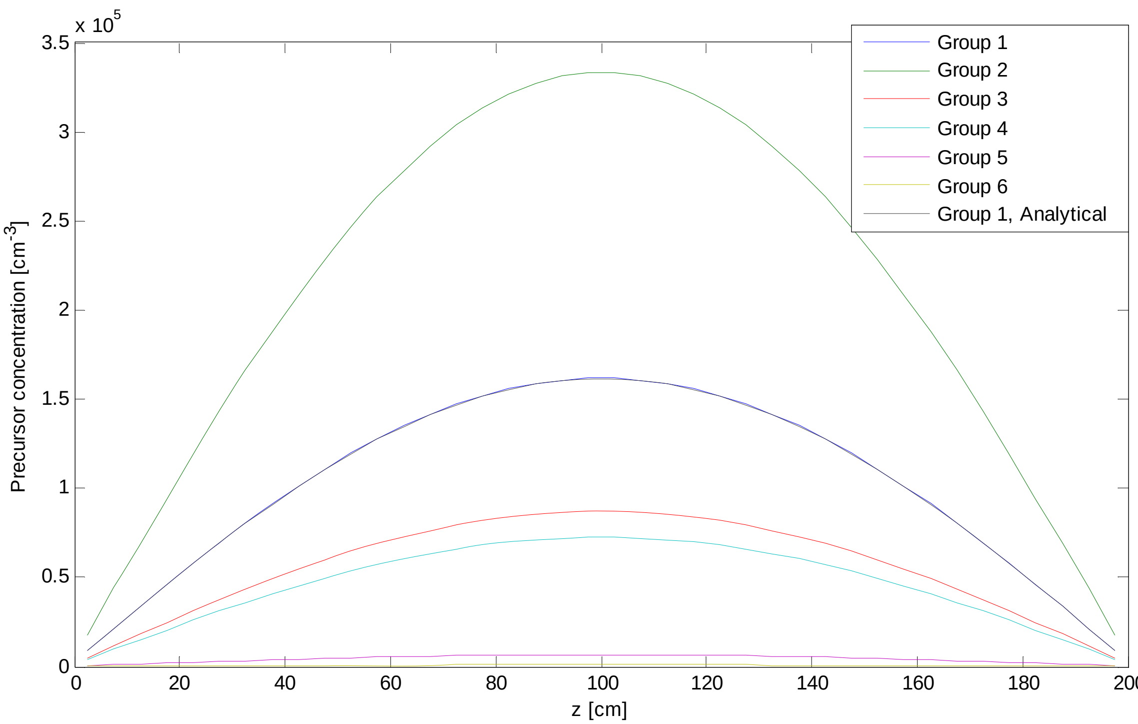

Figure 9.1: Precursor concentrations inside the core for U-235 fuel using JEF precursor decay data as found with the calculation tool and the analytically calculated solution for the first precursor group.

Calculating the precursor concentrations as a function of z of the first precursor group for U-235 fuel with a flat adjoint flux shape and a sine shaped fission shape, using JEF precursor decay data gives ($\Lambda = 2.4 \cdot 10^{-4}$ s, $\lambda_1 = 0.01272$ s^{-1}, $\beta_1 = 25.93 \cdot 10^{-5}$, $A = 4094$ cm^2, $N = 10^9$, $f(z) = \sin\left(\pi\left(z + \frac{1}{2}\lambda_{extrap}\right)/H_{ex}\right) / \int_0^H \sin\left(\pi\left(z + \frac{1}{2}\lambda_{extrap}\right)/H_{ex}\right) dz$, $H_{ex} = 201.95$ cm, $\lambda_{extrap} = 1.95$ cm).

$$C_1(z) = \frac{25.93\cdot 10^{-5}}{2.4\cdot 10^{-4}\cdot 0.01272}\frac{\sin(\pi(z+0.975)/201.95)\cdot 10^9}{4094\cdot\int_0^H \sin(\pi(z+0.975)/201.95)dz}$$
$$= 161411\cdot\sin\left(\frac{\pi\left(z+0.975\right)}{201.95}\right) \qquad (9.1.2)$$

As can be see in figure 9.1, the solution found by the calculation tool and the theoretical solution calculated with 9.1.2 are identical.

9.2 Check of the total number of precursors at steady state with fuel motion.

A test for the correctness of the calculation tool can also be performed for the steady state solution with moving fuel (section 4.1). Taking (2.3.5) and noting that $\varphi^*(z) = 1$, $\int_0^H f(z)dz = 1$, $\partial N/\partial t = 0$ and $\Delta\rho + \beta_{lost} = 0$ gives:

$$\sum_1^6 \lambda_i C_{t,i} = \frac{\beta_{eff} N}{\Lambda} \qquad (9.1.3)$$

with $C_{t,i}$ the total number of precursors of group i. See table 9.1 for the comparison of the analytical results gained from (9.1.3) and the values computed by the calculation tool, with $g = g_{nom} = 80247$ cm^3/s.

Table 9.1: Analytically evaluated $\Sigma(\lambda_i C_{t,i})$ / N compared with the computed values, for the four different neutron data sets ($N = 10^9$).

$\Sigma(\lambda_i C_{t,i}) / N$	U-233		U-235	
	JEF	ORNL	JEF	ORNL
Computed	8.1575	7.2345	30.669	27.754
Analytical	8.1575	7.2345	30.669	27.754

9.3 Check of the effect of the convective term on the precursor concentrations

It was checked if the total number of precursors still stayed correct with fuel flow on. At the start of this test, the precursor concentration was set at $C_{i,j}(z) = 1000$ for all j inside the core and the precursor concentration outside the core was zero. The precursor decay was set to zero ($\lambda_i = 0$). The total number of neutrons N was also kept at zero during the whole test, to prevent precursors from being created.

Two things were tested. In the first place it was tested if the convective term was implemented correctly in the calculation of the precursor concentration, by checking if the total number of precursors stayed the same with fuel flow set to nominal flow rate g = 80247 cm^3/s. The amount of numerical diffusion was also investigated by looking at the speed at which the initial peek of the precursors was smeared out over the primary loop. The test was performed with a time step of Δt = 0.1 s and for a total time of t_{max} = 100 s. The total transit time of the fuel salt in the loop is = 25.19 s with nominal flow speed.

The total number of precursors of group i at t = 0 is $C_i(0)A_{core}ncore\Delta z$ = 1000*4080*5*40 = 8.16*10^8 precursors. The total number of precursors at the end of the test at t = 100 s was (as calculated by the computational tool) SUM(C(i,:)*A(:)*dz) = 8.16000*10^8. The total number of precursors stays exactly the same without precursor decay or creation, so no precursors were lost or created by the flow model.

The precursor concentrations during the test at times t = 0, 10, 30, 60, 100 s are plotted in figure 9.2 as a function of space to gain an insight in the amount of numerical diffusion in the computational tool. Instead of the z-position, the concentrations were plotted against the 'volume' position. This is the amount of volume in the primary loop in the length 0 to z. This is the integral of the cross-section over z: $\int_0^z A(z)dz$. This was done to gain a plot with constant differentials and make it easier to see the numerical dispersion.

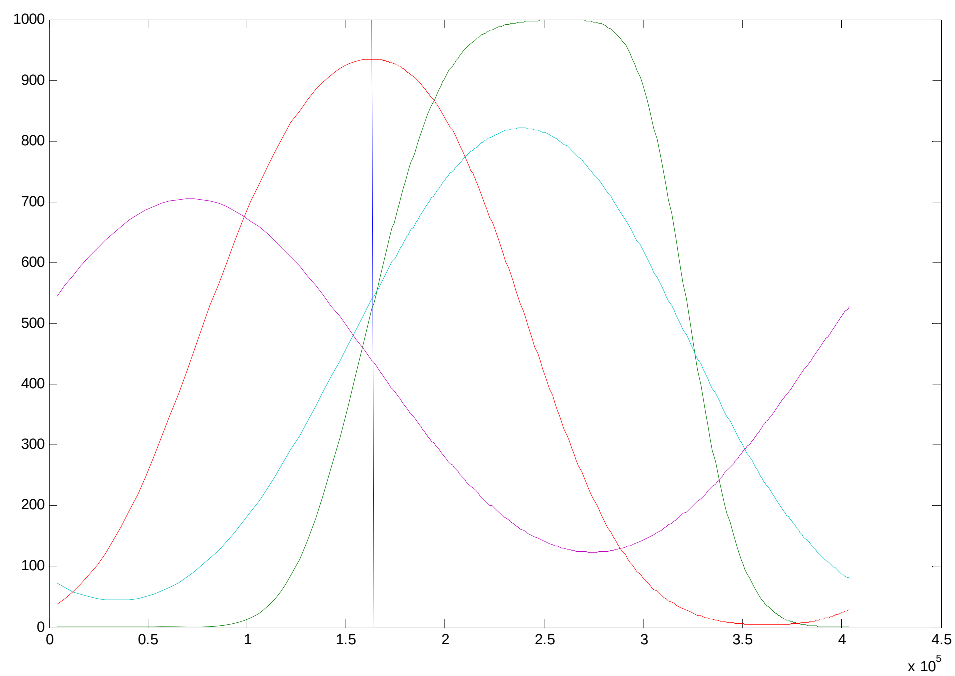

Figure 9.2: Precursor concentrations (#/cm^3) set out against the relative "Volume position". For different times: t=0 s (blue), t=10 (green), t=30 (red), t=60 (cyan), t=100 s (purple), with no decay in time of the precursor.